Electronic Supplementary Information

Energy transfer booster: How a leaving group controls the excited state pathway within a caging BASHY-BODIPY dyad †

Yagmur Aydogan-Sun,[‡a] Maximiliane Horz,[‡b] Rebekka Weber,[c] Myron Heinz,[b] Markus Braun,[a] Alexander Heckel,[*c] Irene Burghardt,[*b] Josef Wachtveitl,[*a]

Content

1. Chemicals and Instruments

All reagents were provided by commercial suppliers like *Sigma Aldrich*, *TCI*, *Alfa Aesar, Acros Organics* or *VWR*) and used without further purification. If not stated otherwise, reactions were performed under argon atmosphere and in dry solvents. Microwave reactions were conducted in a *Biotage Initiator EXP EU* microwave system using sealed microwave vials. Control of the reaction progress was monitored by TLC using silica 60 aluminium sheets with fluorescence indicator UV_{254} from *Macherey-Nagel*. Detection was carried out with UV-light at the wavelengths 254 nm and 366 nm. Crude products were purified by column chromatography either manually with silica gel 60 from *Macherey-Nagel* or automated by flash chromatography with a *PuriFlash XS 420* device and appropriate silica gel columns (30 µm or 50 µm) from *Interchim*. HPLC analysis was performed with an *Agilent 1260 Infinity* device using a *MultoKrom 100-5 250x4.6 mm C18* column.

For the NMR spectroscopic analysis, a 500 MHz device from *Bruker* was used. Samples were prepared using deuterated solvents by *euriso-top*. Spectra were analysed using *TopSpin™* software by *Bruker*. The chemical shift of ^{1}H and $^{13}C\{^{1}H\}$ spectra was calibrated with solvent signal of $CDCl_3$ (δ (ppm) = 7.26 for ^{1}H and 77.16 for $^{13}C\{^{1}H\}$). $SiMe_4$ served as external standard for ^{1}H and $^{13}C\{^{1}H\}$ spectra, while $BF_3{\cdot}OEt_2$ was used for $^{11}B\{^{1}H\}$ spectra and $CFCl_3$ was used for ^{19}F spectra. Electrospray ionisation mass spectrometry (ESI-MS) was conducted at a *Surveyer MSQ plus* device from *Thermo Electron Corporation*, while high-resolution mass spectra (HRMS) were obtained from a MALDI *LTQ Orbitrap XL* instrument from *ThermoScientific*.

2. Synthesis

BODIPY **1**[1] and BASHY **2**[2] were synthesized according to literature.

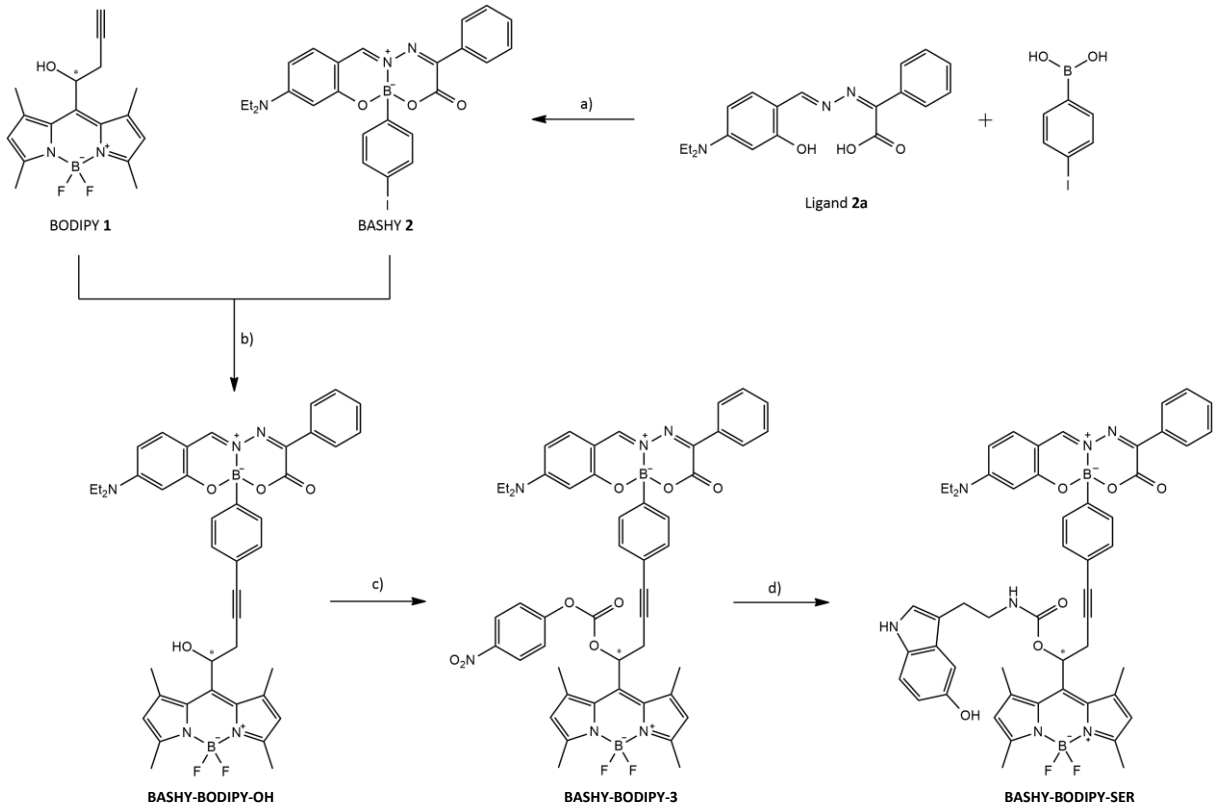

Scheme S1. Synthetic route of the formation of *BASHY-BODIPY-OH* and *BASHY-BODIPY-SER*. a) Ligand *2a*, 4-(iodophenyl)boronic acid, ACN, 80 °C, 3 h, 99%; b) BODIPY *1*, BASHY *2*, $Pd(PPh_3)_4$, CuI, DIPA, THF, 60 °C, 1.5 h, 59%; c) 4-nitrophenyl chloroformate, DMAP, THF/ACN, 50 °C, 3 h (mw), n.d.; d) serotonin hydrochloride, DIPEA, DMF, 50 °C, 75 min (mw), 40%.

BODIPY 1

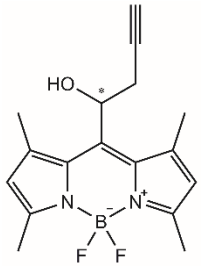

$C_{17}H_{19}BF_2N_2O$

MW = 316.15 g/mol

A suspension of preactivated zinc chips (284 mg, 4.4 mmol, 4.0 eq.) in 5 ml DMF was cooled to 0 °C. After addition of propargyl bromide (124 µl, 1.6 mmol, 1.5 eq.) the mixture stirred for 1 h in the cold. 8-formyl-1,3,5,7-tetramethyl-pyrromethen-fluoroborate (300 mg, 1.1 mmol, 1.0 eq.) was added in 10 ml DMF and the reaction continued stirring for 2 h while warming up to room temperature. The reaction was quenched with saturated NH_4Cl solution and extracted three times with DCM. The combined organic layers were washed with brine, dried over $MgSO_4$ and concentrated *in vacuo*. The residue was purified by column chromatography using cyclohexane/ ethyl acetate (CH/EE (2/1): R_f = 0.40) as eluent to obtain BODIPY **1** in 89% yield (306 mg, 1.0 mmol) as orange-green solid.

^{1}H NMR (500 MHz, $CDCl_3$): δ = 6.10 (s, 2H), 5.70 (dd, J_1 = 10.1 Hz, J_2 = 3.8 Hz, 1H), 3.03 – 2.95 (m, 1H), 2.69 – 2.62 (m, 1H), 2.52 (s, 6H), 2.50 (s, 6H), 2.18 (t, J = 2.7 Hz, 1H) ppm.

^{13}C{^{1}H} NMR (126 MHz, $CDCl_3$): δ = 155.9, 143.5, 130.9, 123.3, 79.8, 71.9, 66.9, 29.7, 26.8, 18.4, 14.6 ppm.

^{11}B{^{1}H} NMR (160 MHz, $CDCl_3$): δ = 0.48 (t, J = 32.4 Hz) ppm.

^{19}F NMR (471 MHz, $CDCl_3$): δ = -146.2 (q, J = 33.1 Hz) ppm.

MALDI-HRMS: *m/z* calcd for $C_{17}H_{19}BF_2N_2O$ [M·]: 316.15530, found 316.15543 (Δm = 0.00013).

BASHY 2

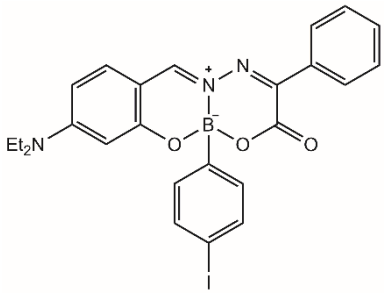

$C_{25}H_{23}BIN_3O_3$

MW = 551.18 g/mol

Ligand **2a** (180 mg, 0.53 mmol, 1.0 eq.) was dissolved in 5 ml ACN. After addition of 4-(iodophenyl)boronic acid (131 mg, 0.53 mmol, 1.0 eq.) the reaction mixture stirred for 3 h at 80 °C. The solvent was removed *in vacuo* and the crude product was purified by column chromatography using cyclohexane/ ethyl acetate (CH/EE (2/1): R_f = 0.37) as eluent to obtain BASHY **2** in 99% yield (289 mg, 0.53 mmol) as yellow solid.

^{1}H NMR (500 MHz, $CDCl_3$): δ = 8.29 (s, 1H), 7.98 (d, *J* = 7.6 Hz, 2H), 7.53 (d, *J* = 7.6 Hz, 2H), 7.46 – 7.37 (m, 3H), 7.21 (d, *J* = 9.1 Hz, 1H), 7.12 (d, *J* = 7.9 Hz, 2H), 6.37 (dd, J_1 = 9.4 Hz, J_2 = 2.1 Hz, 1H), 6.18 (d, *J* = 2.0 Hz, 1H), 3.52 – 3.39 (m, 4H), 1.24 (t, *J* = 7.4 Hz, 6H) ppm.

^{13}C{^{1}H} NMR (126 MHz, $CDCl_3$): δ = 161.5, 157.5, 155.7, 154.0, 153.7, 136.8, 134.7, 132.8, 132.6, 131.1, 129.5, 128.4, 118.0, 108.0, 106.5, 98.8, 94.4, 68.3, 45.5, 38.8, 29.8, 12.9 ppm.

^{11}B{^{1}H} NMR (160 MHz, $CDCl_3$): δ = 4.8 (s) ppm.

ESI-MS: *m/z* calcd for $C_{25}H_{24}BIN_3O_3^+$ [M+H$^+$]: 552.10, found 551.83.

BASHY-BODIPY-OH

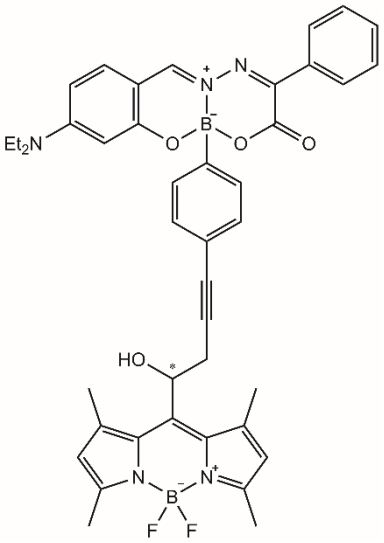

$C_{42}H_{41}B_2F_2N_5O_4$

MW = 739.42 g/mol

BASHY **2** (185 mg, 336 µmol, 1.0 eq.) and BODIPY **1** (191 mg, 604 µmol, 1.8 eq.) were dissolved in 3 ml THF. After addition of $Pd(PPh_3)_4$ (27 mg, 24 µmol, 0.07 eq.), CuI (4.5 mg, 24 µmol, 0.07 eq.) and diisopropylamine (0.5 ml, 3.6 mmol, 11.0 eq.) the mixture was degassed for a few minutes. Then, the reaction was heated in the microwave for 1.5 h at 60 °C. The reaction mixture was poured into water and extracted three times with DCM. The combined organic layers were washed with brine and dried over $MgSO_4$. The solvent was removed *in vacuo* and the crude product was purified by column chromatography using dichlormethane/ ethyl acetate (DCM/EE (30/1): R_f = 0.25) as eluent to obtain **BASHY-BPY-OH** in 59% yield (147 mg, 199 µmol) as orange-red solid.

^{1}H NMR (500 MHz, $CDCl_3$): δ = 8.29 (s, 1H), 7.97 (dd, J_1 = 8.2 Hz, J_2 = 1.7 Hz, 2H), 7.48 – 7.38 (m, 3H), 7.31 (d, J = 8.1 Hz, 2H), 7.25 -7.19 (m, 3H), 6.38 (dd, J_1 = 9.2 Hz, J_2 = 2.4 Hz, 1H), 6.20 (d, J = 2.4 Hz, 1H), 6.07 (s, 2H), 5.70 (dd, J_1 = 9.2 Hz, J_2 = 4.9 Hz, 1H), 3.55 – 3.35 (m, 4H), 3.19 – 3.11 (m, 1H), 2.88 – 2.83 (m, 1H), 2.51 (s, 6H), 2.50 (s, 6H), 1.27 – 1.22 (m, 6H) ppm.

^{13}C{^{1}H} NMR (126 MHz, $CDCl_3$): δ = 157.5, 155.8, 154.8, 153.7, 134.7, 131.0, 130.9, 129.6, 128.4, 123.3, 122.1, 107.9, 106.4, 98.8, 67.3, 45.6, 29.8, 28.2, 22.8, 14.8, 12.9 ppm.

^{11}B{^{1}H} NMR (160 MHz, $CDCl_3$): δ = 0.49 (t, J = 33.0 Hz) ppm.

^{19}F NMR (471 MHz, $CDCl_3$): δ = -146.3 (q, J = 33.0 Hz) ppm.

MALDI-HRMS: *m/z* calcd for $C_{42}H_{41}B_2F_2N_5NaO_4^+$ $[M+Na]^+$: 762.4271, found 762.2817 (Δm = 0.1454).

BASHY-BODIPY 3

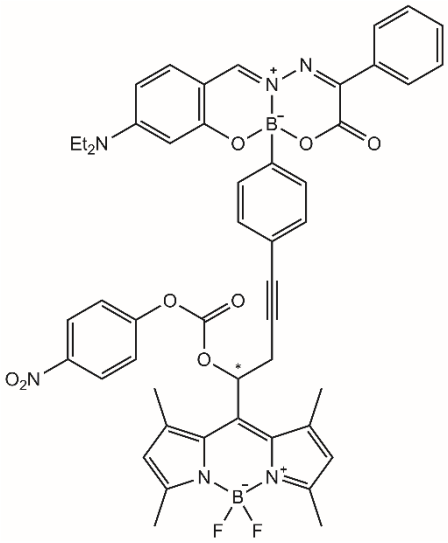

$C_{49}H_{44}B_2F_2N_6O_8$

MW = 904.53 g/mol

BASHY-BODIPY-OH (46 mg, 62 µmol, 1.0 eq.), 4-nitrophenyl chloroformate (38 mg, 189 µmol, 3.0 eq.) and DMAP (9.1 mg, 75 µmol, 1.2 eq.) were dissolved in a mixture of 2 ml THF and 1 ml ACN. The reaction was heated to 50 °C for 3 h in the microwave. The crude reaction mixture was purified by column chromatography using cyclohexane/ ethyl acetate (CH/EE (1/1): R_f = 0.56) as eluent to obtain BASHY-BPY **3** in 60% yield (34 mg, 37 µmol) as orange-red solid. The compound was used without further analysis.

BASHY-BODIPY-SER

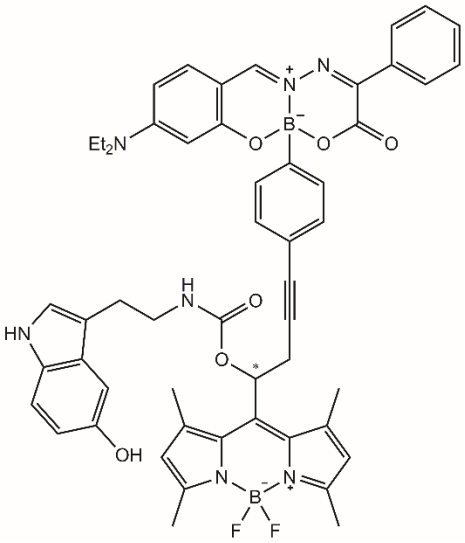

$C_{53}H_{51}B_2F_2N_7O_6$

MW = 941.63 g/mol

BASHY-BODIPY 3 (34 mg, 38 µmol, 1.0 eq.), serotonin hydrochloride (12 mg, 56 µmol, 1.5 eq.) and DIPEA (20 µl, 112 µmol, 3.0 eq.) were dissolved in 3 ml DMF. The reaction mixture was heated to 50 °C for 75 min in the microwave. The crude reaction mixture was purified by column chromatography using cyclohexane/ ethyl acetate (CH/EE (1/1): R_f = 0.18) as eluent to obtain **BASHY-BODIPY-SER** in 40% yield (14 mg, 15 µmol) as orange-red solid.

^{1}H NMR (500 MHz, $CDCl_3$): δ = 8.28 (d, *J* = 5.9 Hz, 1H), 7.96 – 7.92 (m, 2H), 7.69 (br s, 1H), 7.43 – 7.40 (m, 1H), 7.38 – 7.34 (m, 2H), 7.32 – 7.28 (m, 2H), 7.21 – 7.14 (m, 4H), 7.09 (d, *J* = 8.6 Hz, 1H), 6.87 (s, 1H), 6.78 – 6.68 (m, 3H), 6.37 – 6.33 (m, 1H), 6.18 – 6.11 (m, 1H), 6.07 (d, *J* = 4.9 Hz, 1H), 6.03 (s, 1H), 4.75 – 4.68 (m, 1H), 3.48 – 3.33 (m, 7H), 3.18 – 3.10 (m, 1H), 2.93 – 2.88 (m, 1H), 2.82 – 2.76 (m, 2H), 2.64 (s, 3H), 2.50 (s, 6H), 2.34 (d, *J* = 3.6 Hz, 3H), 1.21 (t, *J* = 7.1 Hz, 6H) ppm.

^{13}C{^{1}H} NMR (126 MHz, $CDCl_3$): δ = 161.5, 157.5, 156.0, 154.1, 153.7, 149.7, 134.7, 132.6, 130.8, 129.6, 128.4, 123.7, 123.4, 112.0, 108.0, 106.4, 103.1, 98.8, 67.7, 45.5, 41.3, 36.6, 29.8, 26.3, 25.5, 22.8, 18.5, 18.0, 14.9, 14.7, 12.8 ppm.

^{11}B{^{1}H} NMR (160 MHz, $CDCl_3$): δ = 0.51 (t, *J* = 32.3 Hz) ppm.

^{19}F NMR (471 MHz, $CDCl_3$): δ = -146.1 (q, *J* = 32.4 Hz) ppm.

3. Experimental details

Steady-state absorption experiments

Absorption spectra were recorded with a spectrometer (Specord S600, Analytic Jena, Germany) before and after each experiment to check for any sample degradation. The illumination experiment (Figure 12 in the main text) was conducted in a 4x10 mm cuvette. The sample was placed in a customized sample holder in such a way, that the optical pathlength was along the 10 mm side and the illumination along the 4 mm side. The customized sample holder is connected to a thermostat (S150, Thermo Fisher Scientific, USA) which ensures a constant temperature of 20°C within the sample. Additionally, the sample was constantly stirred with a magnetic stirrer. For the illumination of the sample a 470 nm LED (M470L3, Thorlabs, USA) was used and set to 50 mW/cm^2. After specific time points (shown in Fig. 12), absorption spectra were recorded. The sample was illuminated for 120 mins in total. Afterwards the obtained spectra were baseline corrected and used for the reabsorption correction of the fluorescence spectra.

Steady-State fluorescence experiments

All fluorescence spectra were taken with a fluorescence spectrometer (FP-8500, Jasco, Germany) in the range from 400 nm to 800 nm. As in the absorption experiments, a 4x10 mm cuvette was used for all fluorescence experiments. The samples were set to an OD below 0.1 to avoid any reabsorption effects. The steady-state fluorescence spectra were obtained with an excitation wavelength of 430 nm. Afterwards the raw spectra were baseline corrected and the wavelength sensitivity of the optical elements as well was the photodiode were taken into account.

Fluorescence quantum yield measurements

The fluorescence quantum yields ϕ_F were determined by using an integrative sphere (ILF-835, Jasco, Germany) which was attached to the same fluorescence spectrometer (FP-8500, Jasco, Germany). The samples were excited at 470 nm and 10 accumulations were done. The obtained fluorescence spectra were compared to the solvent (DMSO) spectrum which was measured under the same conditions. The solvent spectrum mainly consists of stray light from the solvent and cuvette. The raw spectra are corrected the same way as the steady-state fluorescence spectra. Afterwards, the solvent spectrum is subtracted from the sample spectra. Thus, the subtracted spectra result in a negative area for the stray light which resembles the absorbed photons and a positive area for the fluorescence of the samples. Both areas are then integrated and ϕ_F was determined by calculating the ratio between the fluorescence and excitation integrals.

Temperature-dependent fluorescence experiments

The temperature-dependent fluorescence experiments were conducted with the same fluorescence spectrometer (FP-8500, Jasco, Germany). The samples were excited at 430 nm and the spectra were recorded for temperatures between 20 °C and 90 °C. The temperature gradient was chosen to be 2.5 °C. A control experiment was applied where only the peak wavelengths of BASHY and BODIPY were recorded. In this second experiment, after a rise from 20 °C to 90 °C, a reversed temperature setting from 90 °C to 20 °C was applied to verify the reversibility of the temperature induced changes.

2-photon-induced fluorescence experiments

For the 2-photon-induced fluorescence (2PIF) measurements, the samples were excited with a tunable optical parametric amplifier (Orpheus-HP, Light Conversion) which is pumped by a 2MHz carbide laser (CB3-40W, Light Conversion). For the 2PIF experiments, the excitation beam is tightly focused into the sample with a 75 mm lens. Approximately 90° to the excitation pathway, the fluorescence is collected by a second 75 mm lens. After separation from the excitation beam with a bandpass filter, the fluorescence was focused into a detector (PMA Hybrid 07, Picoquant) which is together with the laser's own trigger output connected to a time-tagging electronic (PicoHarp 330, Picoquant) for time-correlated single-photon counting (TCSPC). This allows for a precise recording of 2-photon induced fluorescence transients. Afterwards, the transients were integrated to determine the number of emitted photons. The power dependency was measured at 920 nm within a power range from 10 to 40 mW. The 2-photon excitation spectra were measured between 850 and 1100 nm in 10 nm steps with a power of 30 mW. The sample concentrations were adjusted to be below 0.1 OD to minimize reabsorption effects. Rhodamine B was used as a reference to obtain the 2-photon absorption cross-sections in a relative fashion. Therefore, the following equation was used[3]

$$\delta_S = \delta_R \cdot \frac{\phi_F(R) \cdot c_R \cdot F_S \cdot n_R}{\phi_F(S) \cdot c_S \cdot F_R \cdot n_S} \quad (1)$$

where δ is the 2-photon absorption (2PA) cross-section, ϕ_F the 1-photon fluorescence quantum yield, *c* the concentration, *F* the integrated fluorescence intensity and *n* the refractive index. The indices *S* and *R* refer to sample and reference, respectively. It should be noted that the 1-photon and 2-photon quantum yields are assumed to be the same. The fluorescence quantum yield and the 2PA cross-sections of Rhodamine B in methanol were taken from Makarov *et al.*[3].

Femtosecond UV/vis-pump-probe experiments

The femtosecond transient absorption measurements were conducted with a home-made pump-probe setup. The ultrashort laser pulses (150 fs, 775 nm, 1 kHz) are generated by a Ti:Sa chirped pulse regenerative amplifier (MXR-CPA-iSeries, Clark-MXR Inc., USA). At the start of the setup, the fundamental is separated for pump and probe pulse generation. A two-stage noncollinear optical parametric amplifier (NOPA) was used to generate pulses around 940 nm which were used for sum frequency generation (SFG) to obtain 420 nm pulses. The excitation energy was set to 90 nJ/pulse. The white light continuum pulses for probing the absorption changes were generated in a 5 mm CaF_2 crystal. The obtained white light ranges from 350 to 650 nm and was split for referenced detection to a sample and reference arm. Each arm is equipped with a detection system consisting of a spectrograph (Multimode, AMKO) with a 300 nm blaze and a photodiode array (S8865-64, Hamamatsu Photonics) with a driver circuit (C9118, Hamamatsu Photonics). The pump and probe pulses were set to the magic angle to account for anisotropic effects. The measurements were performed in 1 mm quartz cuvettes where the sample concentration was adjusted to be around 0.5 OD. During the measurements, the sample cuvette was constantly moved to avoid photodegradation. The experimental data were analyzed by the lifetime distribution analysis (LDA) in OPTIMUS[4] which uses a quasi-continuous sum of exponentials to allow a model-independent analysis of the data. More details of the analyze procedure can be found in the respective paper of OPTIMUS[4].

FTIR illumination experiments

The IR illumination experiment was conducted with a FTIR spectrometer (Vertex 80, Bruker) under constant nitrogen flow to minimize contributions from H_2O and CO_2. The spectra were recorded from 4000 cm^{-1} to 900 cm^{-1} with a spectral resolution of 4 cm^{-1}. For the illumination, the 470 nm LED was placed at a distance of around 20 cm from the sample. The beam was extended with a telescope system consisting of a 100 mm and 75 mm lenses before reaching the sample. 47 μL of the sample was embedded in a sandwich cuvette consisting of two CaF_2 windows with a 50 μm (d) spacer in between. The sample was dissolved in DMSO and the OD was set to be 0.7 (A_0) at the excitation wavelength. The sample was illuminated for 3 hours with a LED power (P) of 4 mW while every 60 seconds a spectrum was recorded.

The quantum yield of uncaging could be determined by the time dependent evolution (m) of the CO_2 band around 2337 cm^{-1}. Using the above-mentioned parameters and an extinction coefficient of 1500 M^{-1} cm^{-1} (ε_{Prod}) for CO_2 formation[5] with the following equation, results in an uncaging quantum yield of 0.03%.

$$\phi_{\text{Uncaging}} = \frac{m \cdot V \cdot N_A \cdot h \cdot c}{\varepsilon_{\text{Prod}} \cdot d \cdot P \cdot \lambda \cdot (1 - 10^{-A_0})} \quad (2)$$

FRET calculations

The FRET parameters were calculated according to the program[6] and publication[7] by Peter Nagy, which are based on the commonly used FRET equations. In the following a short introduction to these equations are provided and for more details we refer to the above-mentioned sources. The overlap integral is calculated according to following equation,

$$J = \int F_D(\lambda) \cdot \varepsilon_A(\lambda) \cdot \lambda^4 \mathrm{d}\lambda \quad (3)$$

where $F_D(\lambda)$ is the fluorescence spectrum of the donor with the area underneath normalized to 1, $\varepsilon_A(\lambda)$ is the extinction coefficient of the acceptor and λ^4 is used as wavelength correction.

With the overlap integral J, the orientation factor κ^2, the fluorescence quantum yield of the donor ϕ_D and the refractive index n, the Förster radius R_0 can be calculated.

$$R_0 = \text{const.} \sqrt[6]{J \cdot \kappa^2 \cdot \phi_D \cdot n^{-4}} \quad (4)$$

The constant part in front of the root consists of different physical constants, which can be summarized to one constant value. Depending on the desired unit of R_0, this constant value can slightly vary. With R_0, the transfer efficiency E_{FRET} can be estimated for the actual distance R between the chromophores.

$$E_{\text{FRET}} = \frac{{R_0}^6}{{R_0}^6 + R^6} \cdot \left(\frac{R_0}{r}\right)^6 \quad (5)$$

Additionally, if the excited-state lifetime of the donor τ_D is known, the transfer rate k_T can be calculated.

$$k_T = \frac{1}{\tau_D} \cdot \left(\frac{R_0}{r}\right)^6 \quad (6)$$

For the calculation of the overlap integrals, the spectra in Fig. 10 of the main text were used to determine R_0 for each case using the appropriate fluorescence quantum yield of the donor in the respective solvent. The fluorescence quantum yields in DMSO are provided in Table 1 of the main text. Additionally, to these values, the quantum yield of BASHY in toluene (89%) was used for case A.

For the determination of the FRET rates, the excited-state lifetime of the donor is required. For the excited-state lifetime of BASHY in DMSO, the value (0.7 ns) obtained from the transient spectra was used for case

B. The excited-state lifetimes of BASHY in toluene and BODIPY in DMSO were determined using the above-mentioned, home-built TCSPC setup and are provided in the supplementary spectroscopic data.

4. Theoretical calculations

Electronic structure calculations

All ground state geometries have been optimized using density functional theory (DFT) with the CAM-B3LYP functional and def2-SVP basis as included in the GAUSSIAN 16 program package.[8] Solvent effects of Dimethyl sulfoxide (DMSO) were accounted for using the polarizable continuum model (PCM).[9,10] The obtained minimum structures were consistent throughout the conducted benchmark and were confirmed using the Hessian.

The excited state analysis for BASHY-BODIPY-OH was performed using the time-dependent extension of DFT (TD-DTF) with multiple different functional and basis set combinations (see Tab. S1). Overall CAM-B3LYP, wB97XD, as well as M06 showed a correct state ordering in which the BODIPY-centered state is the S_1 state, the BASHY-centered state is the S_2 state followed by higher-lying BASHY states that display a relatively high two-photon cross-section. The other tested methods (B3LYP and PBE0) either yielded an incorrect state ordering or strongly deviating state energies with states that feature a strong charge transfer character. CAM-B3LYP was chosen for the analysis due to an overall reasonable performance as well as availability in other program packages such as DALTON, which was employed for the quadratic response calculations yielding the two-photon cross-sections.[11]

Table S1. Benchmark of the dyad without leaving group (LG) BASHY-BODIPY-OH including the three excited states of interest, namely the lowest singlet excited state located on the BODIPY fragment and the two excited states localized on the BASHY fragment, one of which is the target state for a possible one-photon excitation and the other being the two-photon active state. Both of the BASHY states display a two-photon activity in general, the mentioned state corresponds to the higher-lying two-photon active state that exhibits the bigger cross-section. Listed are the excitation energy in eV and nm as well as the respective oscillator strength (*f*).

BASHY-BODIPY-OH

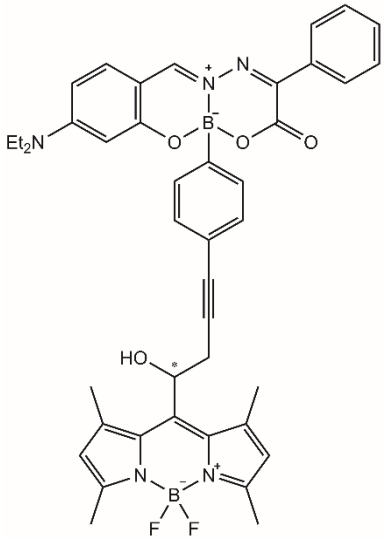

Functional	Basis set	BPY-state	Energy [eV]	Energy [nm]	*f*	BASHY-state	Energy [eV]	Energy [nm]	*f*	BASHY-2P-state	Energy [eV]	Energy [nm]	*f*
CAM-B3LYP	def2-SVP	1	2.8480	435.34	0.5808	2	3.1749	390.52	1.2701	4	3.8412	322.78	0.0887
B3LYP	def2-SVP	4	2.8339	437.50	0.6969	1	2.7523	450.47	0.5602	2	2.7512	449.02	0.3853
M06	def2-SVP	1	2.8167	440.80	0.3232	2	2.8672	432.43	1.4205	4	3.1873	389.00	0.0432
wB97XD	def2-SVP	1	2.8479	435.36	0.5945	2	3.2026	387.13	1.2548	4	3.8499	322.04	0.0845
PBE0	def2-SVP	2	2.8786	430.72	1.1005	1	2.8456	435.70	0.6732	3	2.9985	413.49	0.0056

Rotational potential

As the linear connection between the two combined chromophores imposes a geometry that suggests a small rotational barrier, a relaxed scan around the highlighted carbon atoms C1-C4 in Fig. S1 was conducted to screen for possibly important geometries around the central connection axis within the ground state. As expected, the height of the rotational barrier in case of BASHY-BODIPY-SER is ten times more pronounced than the one of BASHY-BODIPY-OH. In both cases the potential suggests, that all orientations are available at room temperature. To quantify that Boltzmann populations were calculated as depicted in Fig. S1 according to

$$p_i = \frac{1}{Q} \cdot e^{-\frac{E_i}{k_B T}} = \frac{e^{-\frac{E_i}{k_B T}}}{\sum_{i=1}^{N} e^{-\frac{E_i}{k_B T}}} \tag{7}$$

where Q as normalization denominator denotes the canonical partition that sums over all possibly accessible states N with the respective energy E_i.

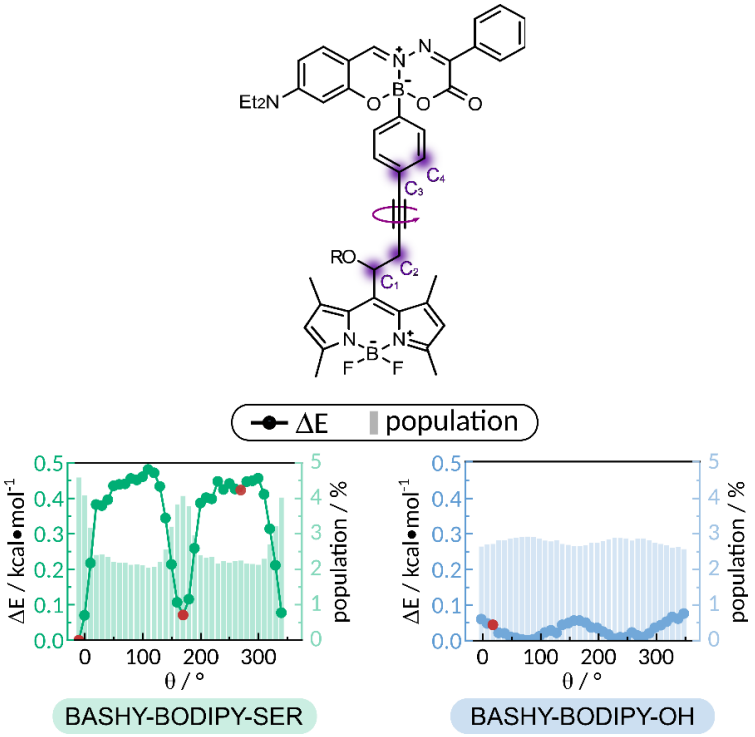

Figure S1. Rotational potential of a relaxed surface scan around the indicated axis of C1-C2-C3-C4 effectively describing a rotation around the linker. The energy is indicated as the difference between the energy of the respective geometry and the lowest lying energy. Boltzmann populations are provided in %. Geometries used for further quantum dynamical analyses are marked in red. Since BASHY-BODIPY-SER displays a slight preference for parallel orientations of the two fragments three representative geometries are included covering different ranges of the distribution. BASHY-BODIPY-OH is represented with one geometry approximately comparable to the one corresponding to the lowest point in BASHY-BODIPY-SER.

As the rotational PES scan revealed slight preferences in case of BASHY-BODIPY-SER three different geometries were chosen as representation for the later analysis, covering the two minima displayed in Fig. S1 corresponding to a nearly parallel orientation of the two chromophores ($\Theta \approx 0°$ and $\Theta \approx 180°$) and one of the slightly less populated perpendicular geometries ($\Theta \approx 270°$). The structures associated with the marked geometries of BASHY-BODIPY-SER are given in Fig. S2 ordered accordingly.

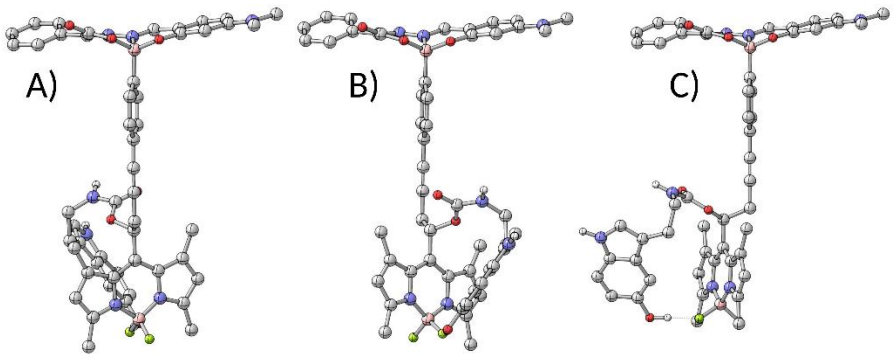

Figure S2. Geometries corresponding to the highlighted red orientations of BASHY-BODIPY-SER in Fig. S1. A) belongs to the first point at approximately $\Theta \approx 0°$, B) to the second one at about $\Theta \approx 180°$ and C) corresponds to the third geometry highlighted in the scan ($\Theta \approx 270°$).

The two minima, as expected, seem to be mirror images while the third geometry displays a nearly perpendicular alignment of the dyad compounds. The BASHY geometry seems to be rather robust throughout the rotation.

Excited state analysis

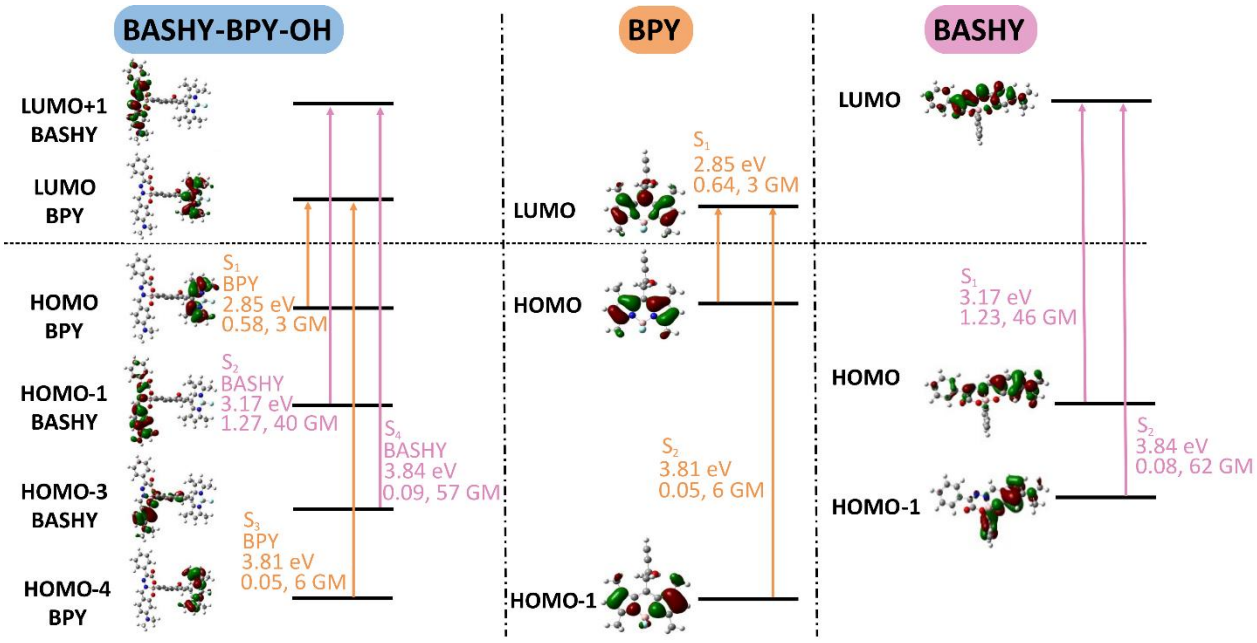

Figure S3. Frontier molecular orbital transitions involved, excitation energies with oscillator strength and two-photon absorption cross-sections of the four first excited singlet states of BASHY-BODIPY-OH in comparison to the respective properties of the individual fragments BODIP (BPY) and BASHY at CAM-B3LYP/def2-svp level in DMSO.

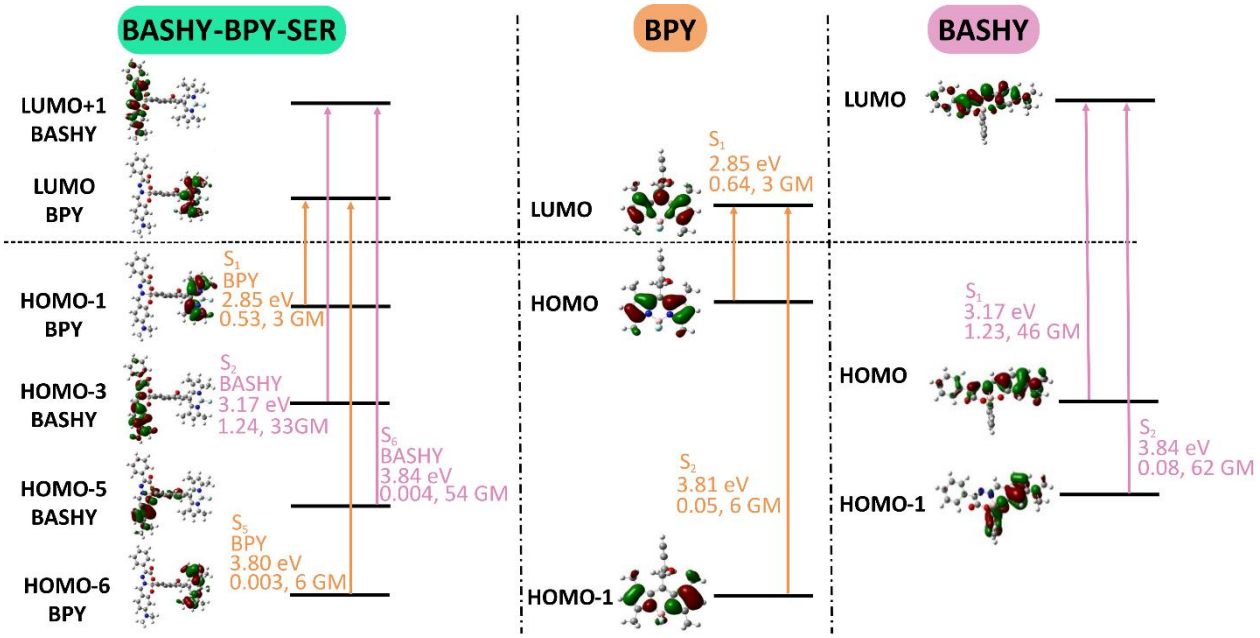

Figure S4. Frontier molecular orbital transitions involved, excitation energies with oscillator strength and two-photon absorption cross-sections of the four excited singlet states of interest within the BASHY-BODIPY-SER dyad in comparison to the respective properties of the individual fragments BODIP (BPY) and BASHY at CAM-B3LYP/def2-svp level in DMSO.

Intramolecular charge transfer (ICT) character BASHY

The intra fragment ICT character of the BASHY-centered excited state of the dyads (here illustrated on the BASHY-BODIPY-OH dyad) is caused by a planarization of the ring with regard to the rest of the big $\pi-$ system.

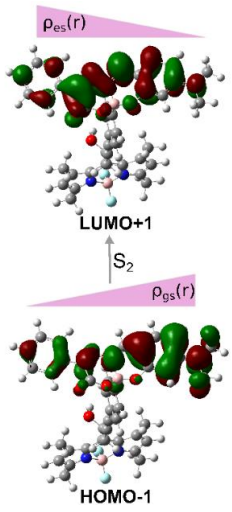

Figure S5. Frontier molecular orbital transition at CAM-B3LYP/def2-SVP level in DMSO illustrating the shift of electron density within the S_2 state transition. Both dyads display the ICT character upon planarization of the π-system in the excited state.

Natural transition orbitals (NTO) for BASHY

Since the BASHY-centered states display an ICT character the NTOs are displayed in addition to the canonical molecular orbitals to underline that the transitions can be described by a HOMO→LUMO transition that exhibits a π→π* character. As they provide a more intuitive and sometimes clearer picture of a hole-electron excitation the NTO transition for the first and second BASHY-centered state (S_2 and S_4 state for BASHY-BODIPY-OH and S_2 and S_6 state for BASHY-BODIPY-SER) are supplied in the following.

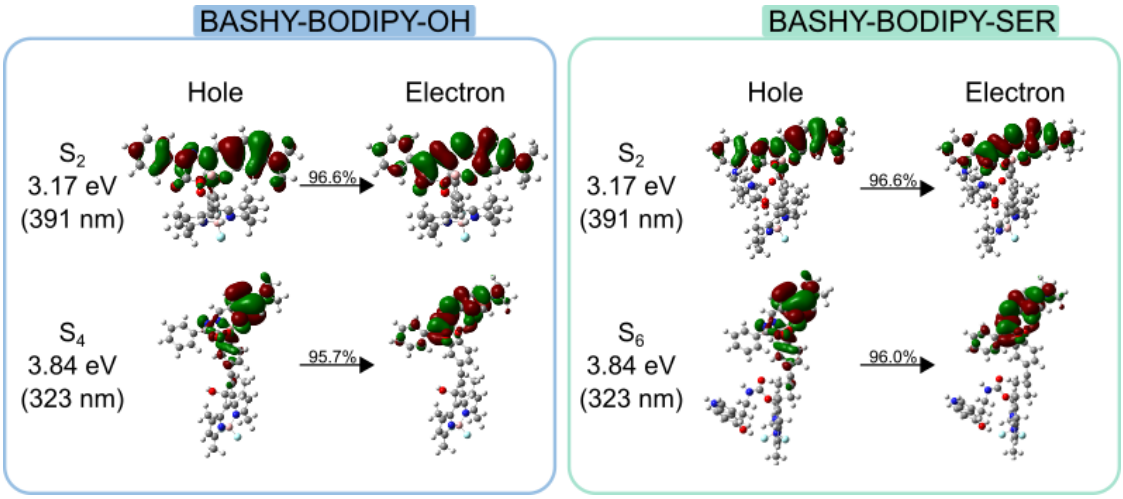

Figure S6. NTOs for the relevant BASHY-centered excited states with the respective excitation energies for BASHY-BODIYP-OH and BASHY-BODIPY-SER.

ICT analysis

The examination of the ICT character of the excited states was conducted employing an analysis of the descriptors $\Omega_{AB}^{\mathrm{nm}}$ ('Ω matrix') with the initial state n and the final state m for the molecular fragments A and B. This analysis was carried out using the TheoDORE tool.[12,13] Conceptually the evaluation is based on the picture of a correlated electron-hole pair and utilizing one-particle transition density matrices in combination with a suitable partitioning of molecular fragments, that is discussed in the next section. The one-particle transition density reads

$$\gamma^{n,m}(r_h, r_e) = n \int \psi^n(r_h, r_2, \dots, r_n)\psi^m(r_e, r_2, \dots, r_n)\, \mathrm{d}r_2 \dots \mathrm{d}r_n \qquad (8)$$

with r_h and r_e specifying the coordinates of hole and electron, respectively. n = 0 refers to a transition from the ground state. The descriptor $\Omega_{AB}^{\mathrm{nm}}$ is then obtained as[14]

$$\Omega_{AB}^{\mathrm{nm}} = \frac{1}{2}\sum_{\substack{a\in A\\ b\in B}} \left(\boldsymbol{\gamma}^{n,m,[\mathrm{AO}]}\boldsymbol{S}^{[\mathrm{AO}]}\right)_{ab}\left(\boldsymbol{S}^{[\mathrm{AO}]}\boldsymbol{\gamma}^{n,m,[\mathrm{AO}]}\right)_{ab} \tag{9}$$

where $\boldsymbol{S}^{[\mathrm{AO}]}$ denotes the overlap integral in the atomic orbital (AO) basis while *A* and *B* refer to fragments of the molecule and *a* and *b* label AO indices. The amount of ICT (ICT number in Tab. 2 of the main text) from fragment *A* to fragment *B* is computed as the sum over Ω_{AB}^{nm} (for $A \neq B$); the contribution of the excitation on the same fragment is given by $\Omega_{AA}^{\mathrm{nm}}$. Hence, the ICT character is defined by summing over the off-diagonal elements, yielding[14]

$$\text{ICT number} = \frac{1}{\sum_{AB}\Omega_{AB}^{nm}}\sum_{A}\sum_{A\neq B}\Omega_{\mathrm{AB}}^{nm} \tag{10}$$

This corresponds to the total weight of configurations where the initial and final orbitals are localized on different fragments.

Partitioning of BASHY-BODIPY within the TheoDORE analysis

The previously discussed ICT analysis presumes the division of the system in sub-fragments. For both BASHY-BODIPY systems these fragments are defined according to the units employed for the initial synthesis. This leaves us with three sub-units of BASHY approximately corresponding to the salicylidene hydrazone (1), the α-keto acid scaffold (2) as well as the backbone of the boronic acid (3). Additionally, the bridge (4) as well as the BODIPY chromophore (5) are defined as fragments. This partitioning is utilized for both dyads, BASHY-BODIPY-OH as well as BASHY-BODIPY-SER and illustrated in Fig. S7.

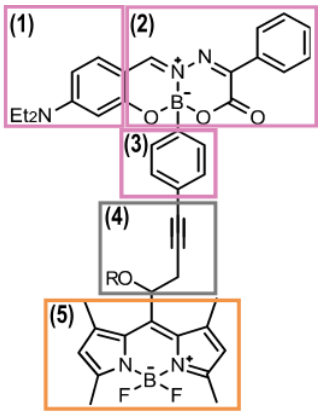

Figure S7. Fragments used for the TheoDORE analysis of the BASHY-BODIPY-OH and BASHY-BODIPY-SER dyad. Affiliation to either BASHY or BODIPY is indicated by pink and orange boxes, respectively. Ascending numbering corresponds to the designation in the text above.

Excited state scan connecting FC and S_3 state minimum

As the shape of the excited state surfaces play a pivotal role in the explanation of the difference in efficiency of the energy transfer between the two chromophores, extensive scans of the S_1 and S_2 state surfaces were conducted within the limitations of a high-dimensional system, see Fig. 7 of the main text. The optimization of the S_1 state revealed two possible minima, where one can be traced back to the S_1 state at the FC point and thus relates to the investigated BODIPY-centered state of the suggested excitation scheme (S_1^+ state in Fig. 7 in the main text) while the other corresponds to the minimum of a state that is originally the S_3 state at the FC geometry. As this state might be involved in the later uncaging pathway, and to provide a complete picture the scan from the FC geometry to the optimized geometry of the S_3 state is depicted in Fig. S8. This is a rigid scan following the scanning coordinate *X* and thus the gradient of the S_3 state. The increments of the coordinate are normalized and the step size is chosen small enough to reasonably assume we are following the minimum energy pathway (MEP). $X = 0$ corresponds to the FC geometry, while $X = 1$ describes the optimized S_3 state geometry. The excited state minimum in question corresponds to the S_1^- state depicted in Fig. 7 of the main text.

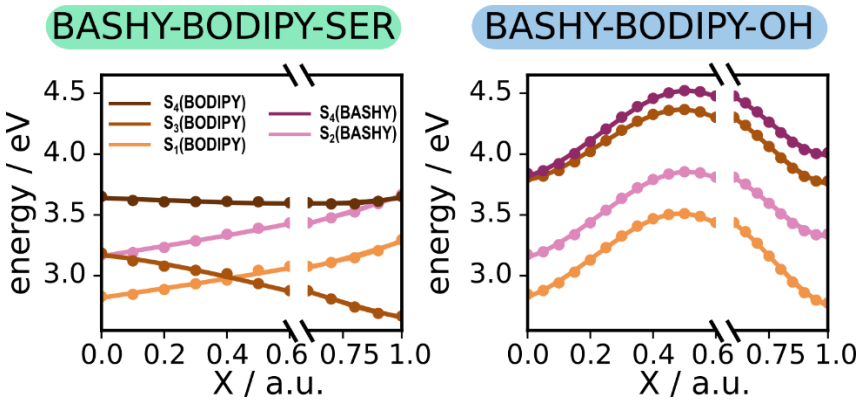

Figure S8. Potential energy surface scan from the FC geometry to the S_3 state minimum thus featuring the transfer of electron density from the BOIDPY fragment to the leaving group serotonin for BASHY-BODIPY-SER. Characteristics like localization on a specific fragment are indicated with orange (BODIPY) and pink (BASHY) and the adiabatic state labels are given in the color of the respective dyad system.

Molecular movement along ICT^D state relaxation

To better understand the molecular coordinates contributing to the differences in dynamics, the projection of the effective X_1-scanning coordinate onto molecular coordinates is examined in greater detail. Relaxation along the ICT^D state potential involves two key movements. The first is the planarization of the benzyl-substituent in BASHY relative to the extended π-system, characterized by an increase in the torsional angle from approximately 150° to 180°. This motion is depicted in red and labeled as α in Fig. S9. In BASHY-BODIPY-SER, the planarization occurs more rapidly and is largely complete at the crossing of the LE^A and ICT^D states. In contrast, the α coordinate in BASHY-BODIPY-OH remains active beyond this point and progresses more slowly overall.

The second movement, marked in blue as β, involves rotation around the linker axis, which introduces a subtle tilt between the BASHY π-system and the plane defined by the benzyl-substituent linking BASHY and BODIPY. Unlike the first movement, this rotation appears to be largely decoupled from the stabilization of the ICT^D state with regards to the LE^A state, occurring predominantly after the crossing. These distinct movements along α and β highlight similarities but also differences in the relaxation dynamics between the BASHY-BODIPY-SER and BASHY-BODIPY-OH systems.

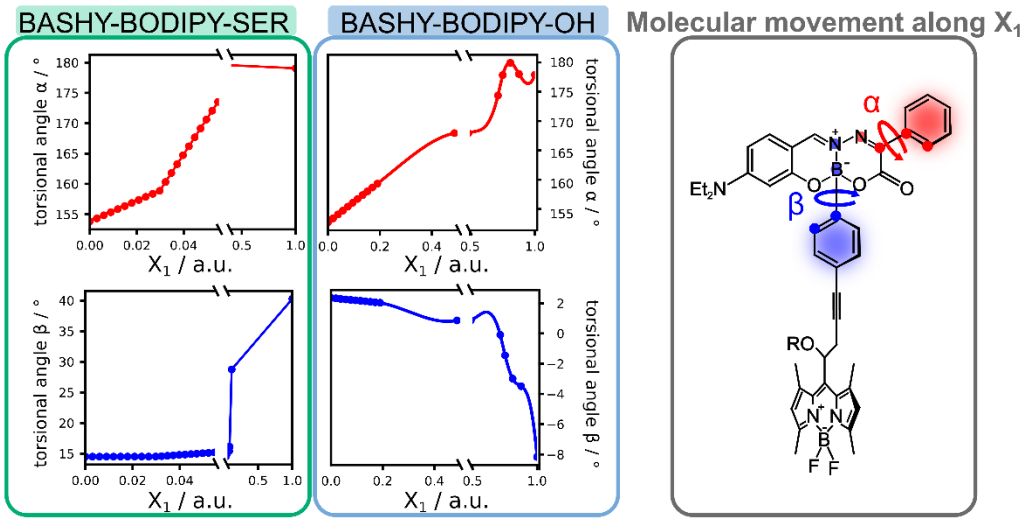

Figure S9. Distinct torsional scans along the effective X_1 coordinate, describing the relaxation in the ICT^D state. The relevant angles α and β are indicated in red and blue, respectively.

Initial condition for quantum dynamical simulations

The initial condition is chosen according to the assumed excitation scheme where the initial excitation is limited to the BASHY-centered one- and two-photon active S_2 state. A possible initial excitation to higher-lying two-photon active states is not considered, but upon inclusion would necessitate to consider internal conversion dynamics. This is also the chosen initial condition for the quantum dynamic simulation. Due to the fragment-wise localization of the respective excited states, this implies that all density is located on the BASHY fragment in the beginning. The localization and resulting small electronic coupling are also the reason why the initially adiabatic state energies were assumed to be feasible as localized excited 'diabatic' state energies LE^A and ICT^D for the dynamics. The initial condition is used for all different geometries as all of them feature the same state ordering and localization.

Linear Vibronic Coupling (LVC) model

The excited state potentials are constructed within a shifted harmonic oscillator model, i.e. the Linear Vibronic Coupling (LVC) model. Thus, the diagonal excited state potentials of all states along the mass- and frequency weighted normal coordinate q_i can be expressed as

$$V_\alpha(q_i) = \frac{1}{2}\omega_i\left(q_i - q_{i,0}^{(\alpha)}\right)^2 + \Delta E$$
$$V_\alpha(q_i) = \frac{1}{2}\omega_i q_i^2 + \kappa_i^{(\alpha)} q_i + d_i + \Delta E \qquad (11)$$

where ω_i is the normal mode frequency, $q_{i,0}^{(\alpha)}$ the shifted minimum of the excited state potential and ΔE the vertical energy offset. The vibronic couplings $\kappa_i^{(\alpha)} = -\omega_i q_{i,0}^{(\alpha)}$ can be computed by projecting the cartesian gradient of the respective state of interest onto the molecular normal modes

$$\kappa_i^{(\alpha)} = \left(\frac{\partial V_\alpha(q)}{q_i}\right)_{q_0} \tag{12}$$

Spectral Densities

The collection of vibronic couplings $\kappa_i(\alpha)$ defines state specific spectral densities.[15]

$$J_\alpha(\omega) = \frac{\pi}{2}\sum_{i=1}^{N} \kappa_i^{(\alpha)2}\, \delta(\omega - \omega_i) \tag{13}$$

These are subsequently convoluted with a Lorentzian broadening with $\tilde{\Delta} = \Delta * 0.2$ where Δ is the root mean square of the frequency differences. In order to calculate the spectral densities of the individual fragments all degrees of freedom of the respective other fragment were frozen in the normal mode calculation.

BASHY-BODIPY-OH

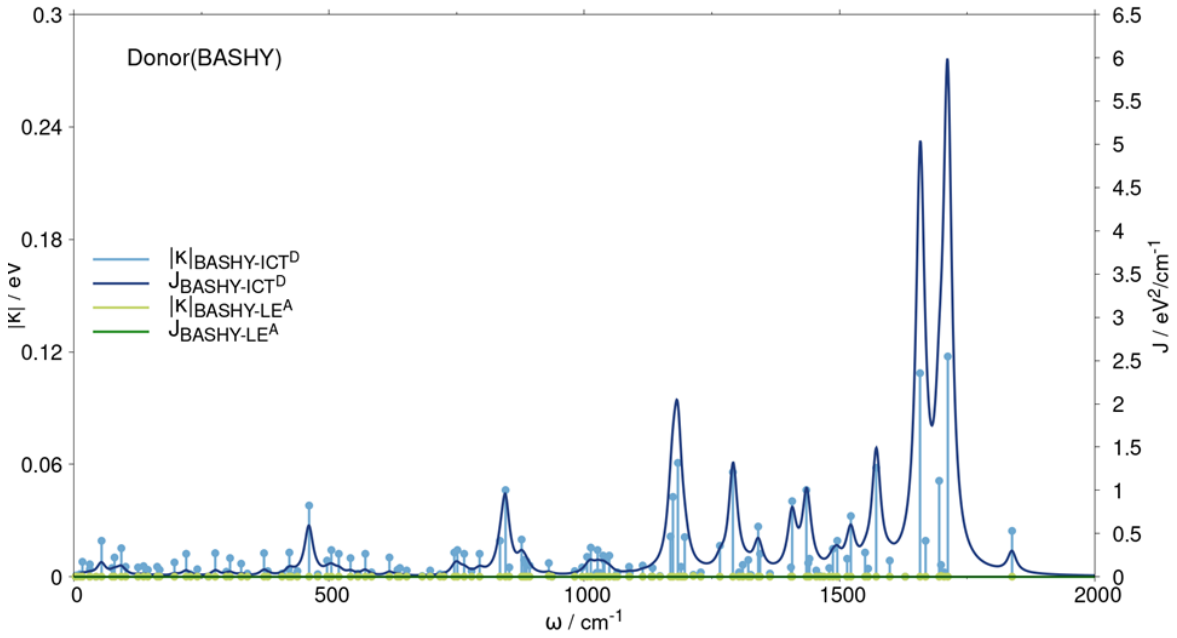

Figure S10. Spectral density J and absolute values of the vibronic couplings $\kappa_i^{(\alpha)}$between the normal modes located on the donor fragment BASHY and the LE^A state (corresponding to the adiabatic S_1 state) and ICT^D state (corresponding to the adiabatic S_2 state), whose orbital transitions are naturally localized on the BODIPY and BASHY fragment, respectively.

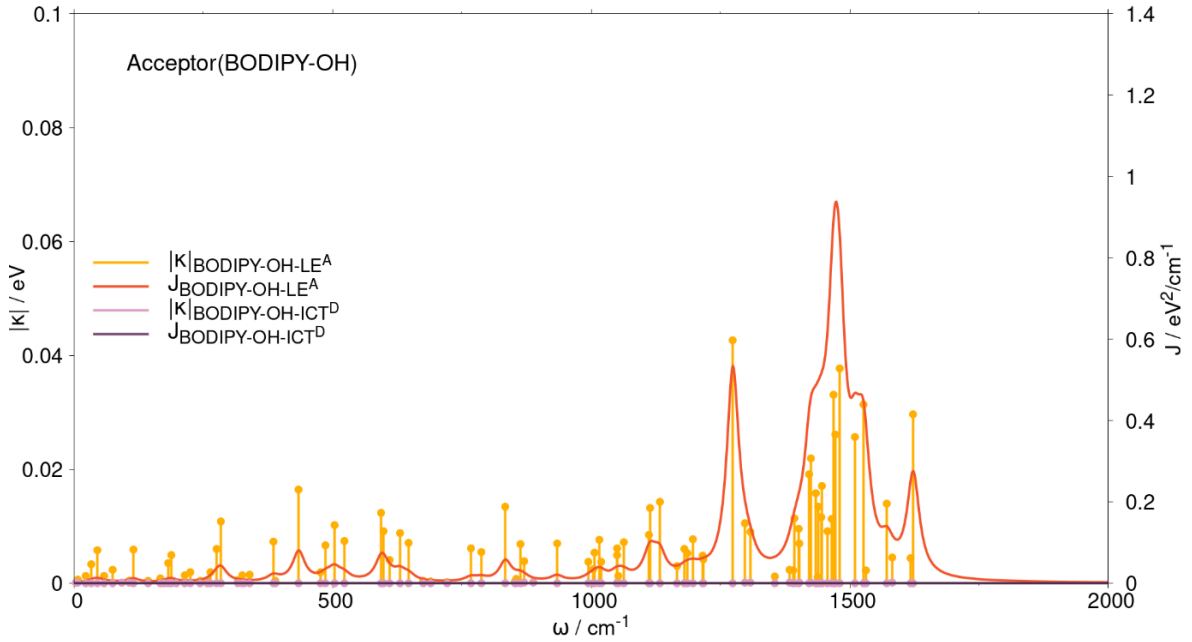

Figure S11. Spectral density J and absolute values of the vibronic couplings $\kappa_i^{(\alpha)}$ between the normal modes located on the acceptor fragment BODIPY and the LE^A state (corresponding to the adiabatic S_1 state) and ICT^D state (corresponding to the adiabatic S_2 state), whose orbital transitions are naturally localized on the BODIPY and BASHY fragment, respectively.

BASHY-BODIPY-SER

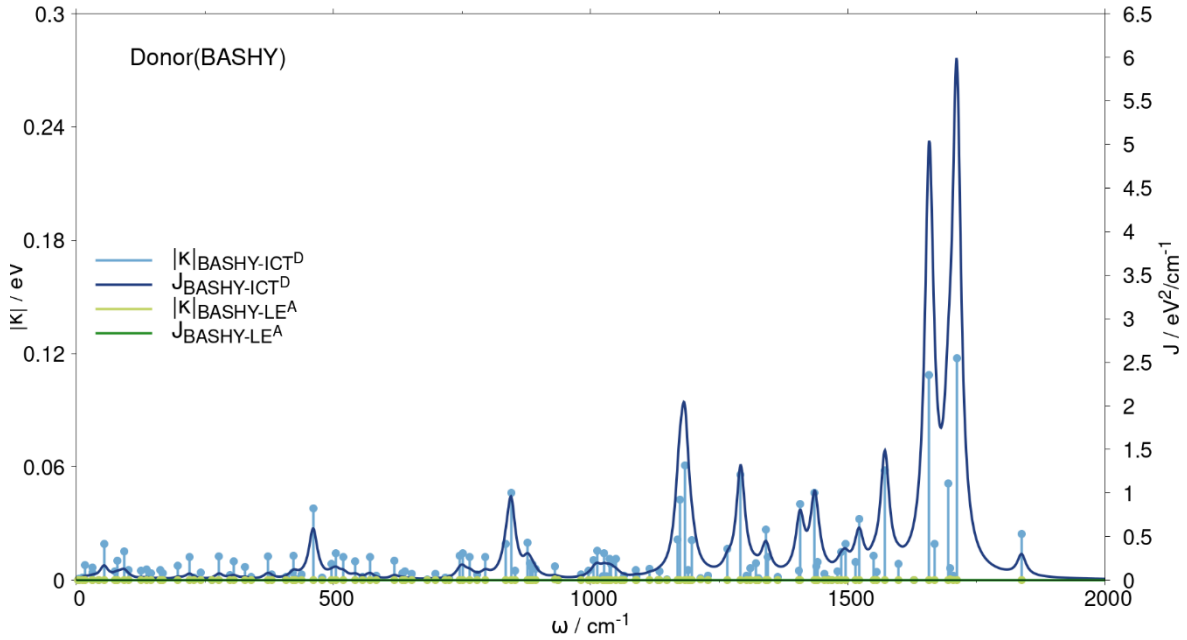

Figure S12. Spectral density J and absolute values of the vibronic couplings $\kappa_i^{(\alpha)}$ between the normal modes located on the donor fragment BASHY and the LE^A state (corresponding to the adiabatic S_1 state) and ICT^D state (corresponding to the adiabatic S_2 state), whose orbital transitions are naturally localized on the BODIPY and BASHY fragment, respectively.

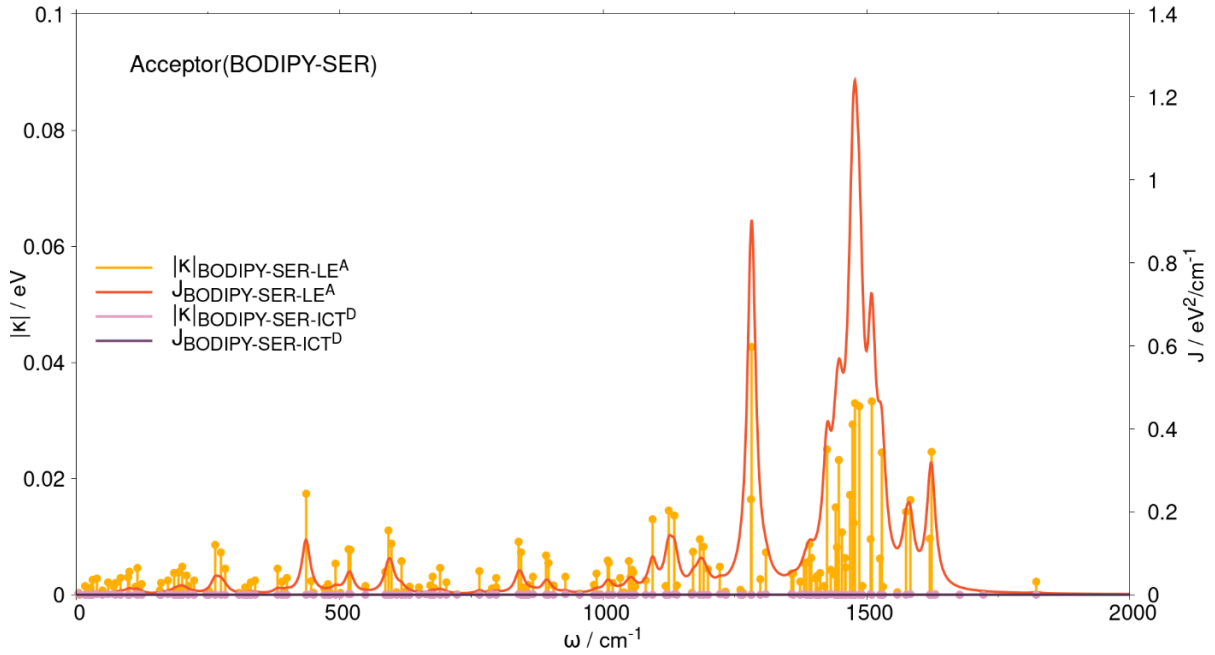

Figure S13. Spectral density J and absolute values of the vibronic couplings $\kappa_i^{(\alpha)}$between the normal modes located on the acceptor fragment BODIPY (including LG serotonin) and the LE^A state (corresponding to the adiabatic S_1 state) and ICT^D state (corresponding to the adiabatic S_2 state), whose orbital transitions are naturally localized on the BODIPY and BASHY fragment, respectively.

Diabatic population

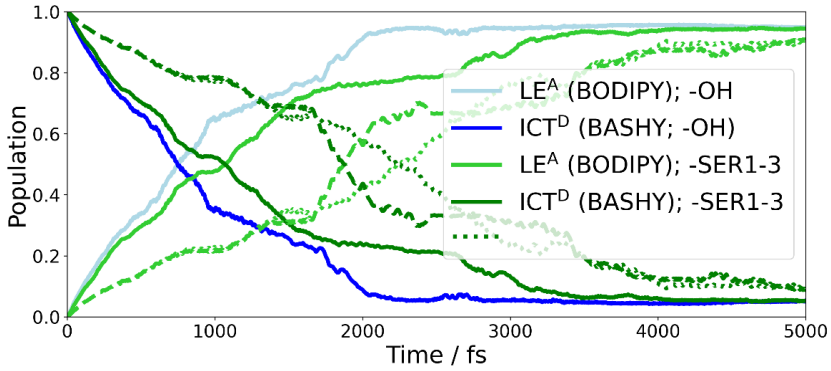

Figure S14. Diabatic population transfer between the two involved LE^A (light colors) and ICT^D state (dark colors) for BASHY-BODIPY-OH (blue) and the three conformations of BASHY-BODIPY-SER (green) depicted in Fig. S1 and Fig. S2. Approximate exponential decay-rates are given in the main text. 1 (solid green) corresponds to geometry Fig. S2A), 2 (dashed green) to Fig. S2B), and 3 (dotted green) to Fig. S2C).

Electronic coherence

The electronic coherence is in general obtained from the density operator $\hat{\rho}(t) = |\psi(t)\rangle\langle\psi(t)|$ of the full vibronic system as

$$\hat{\rho}_{\mathrm{DA}} = \mathbf{Tr}\{\left|\mathrm{LE}^{\mathrm{A}}\right\rangle\left\langle\mathrm{ICT}^{\mathrm{D}}\right|\hat{\rho}(t)\} \tag{14}$$

Its imaginary part corresponds to the transient state-to-state population flux, whereas the real component signifies whether a coherent superposition involving a mixture of both participating states is present.

In contrast to the rapid decay observed in the imaginary part of the electronic coherence of the RHO-BODIPY dyad, both BASHY-based dyads exhibit an oscillatory behavior around zero with a duration of a few picoseconds, during which a built-up coherence decays again almost immediately. Such behavior suggests the possibility of a quasi-kinetic EET mechanism. This is a notable distinction from the preceding rhodamine-based dyad, where the coherence displayed a decay on the timescale of 300-400 fs.

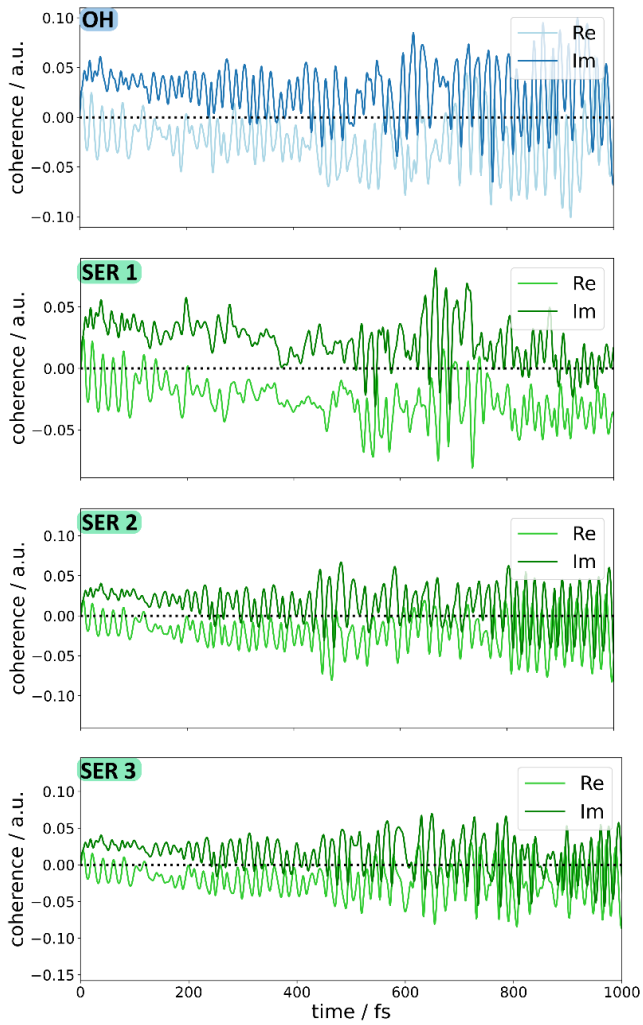

Figure S15. Electronic coherence obtained from the quantum dynamical simulations employing the LVC model for both dyads BASHY-BODIPY-OH and BASHY-BODIPY-SER as well as the three different rotational conformations for the dyad with leaving group (Fig. S2).

The real part not decaying to zero indicates a coherent superposition of the LE^A and ICT^D state, which marks an incomplete transfer that is also visible in the diabatic populations, where between 10-15% remain in the ICT^D state. This is in agreement with previously investigated similarly constructed systems and the experimental time-resolved spectra.

Vibrationally resolved absorption spectra

Vibrationally resolved absorption spectra can be obtained from a quantum dynamical analysis via the Fourier transform of the correlation function and the connection to the power spectrum. The initial condition at the FC geometry $\Psi_g(0)$ is used in order to obtain the absorption cross-section with vibrational resolution[16]

$$\sigma_{\mathrm{Abs}}(\omega) = \frac{2\pi\omega}{3\hbar c}\int_{-\infty}^{\infty} \mathrm{d}t \langle \Psi_{\mathrm{g}}(0)|\Psi_{\mathrm{g}}(t)\rangle e^{(i(E+E_{0,g})t/\tau_{\mathrm{abs}})} \quad (11)$$

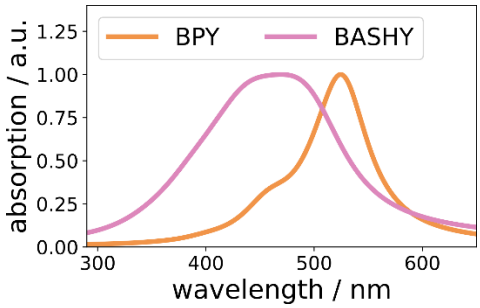

Figure S16. Normalized vibrationally resolved linear absorption spectra for the BASHY fragment (pink) and BODIPY (orange).

5. Supplementary spectroscopic data

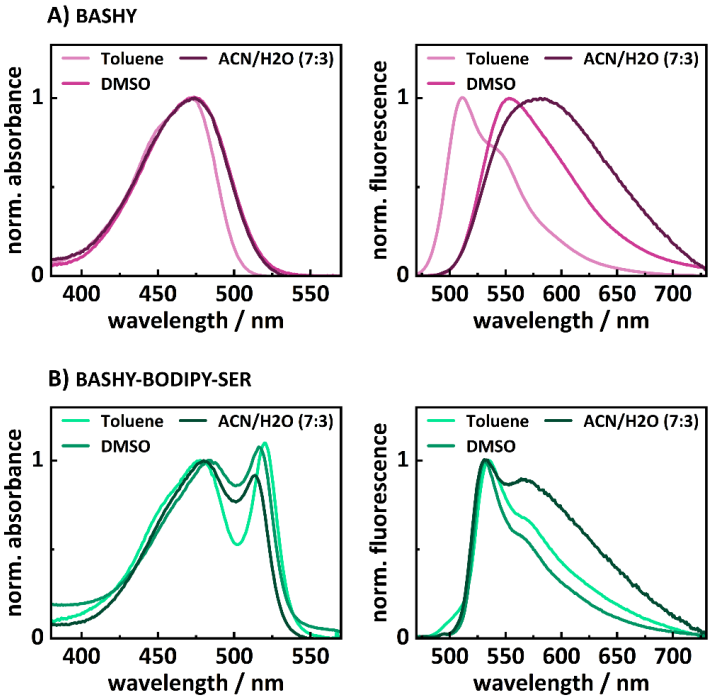

Figure S17. Solvent-dependent absorbance spectra (left) and fluorescence spectra (right) of A) BASHY and B) BASHY-BODIPY-SER.

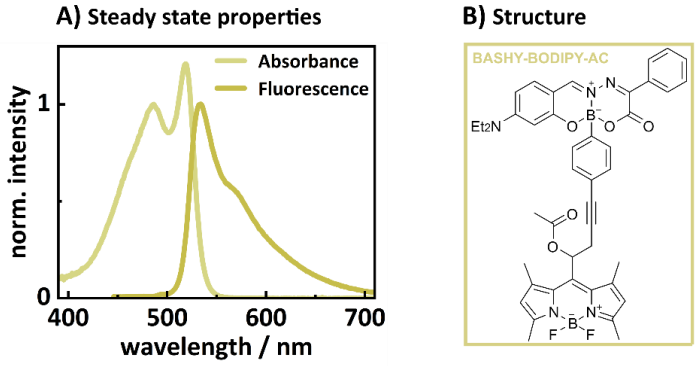

Figure S18. A) Absorbance and fluorescence properties of BASHY-BODIPY-AC in DMSO. B) Chemical structure of BASHY-BODIPY-AC.

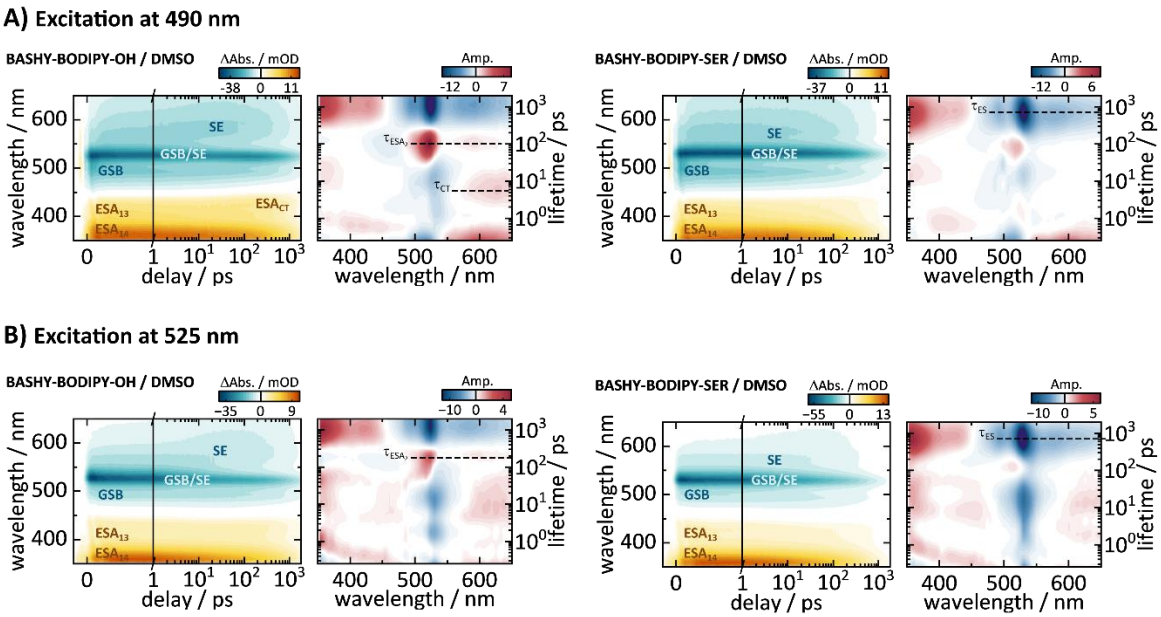

Figure S19. Transient absorption maps with an excitation wavelength of A) 490 nm and B) 525 nm of BASHY-BODIPY-OH (left) and BASHY-BODIPY-SER (right). A 490 nm excitation addresses both chromophores equally, while an excitation at 525 nm mainly addresses BODIPY. As expected, in both excitation cases an energy transfer from BASHY to BODIPY is not observable since BODIPY is directly excited as well. Therefore, the positive amplitude of the energy transfer is replaced by a negative feature from the BODIPY decay. For an excitation at 525 nm, where predominantly BODIPY is excited, no direct evidence for a reverse energy transfer from BODIPY to BASHY is observable. Yet, there is still a significant ESA_2 contribution visible in the LDM of BASHY-BODIPY-OH due to residual BASHY absorption at the excitation wavelength.

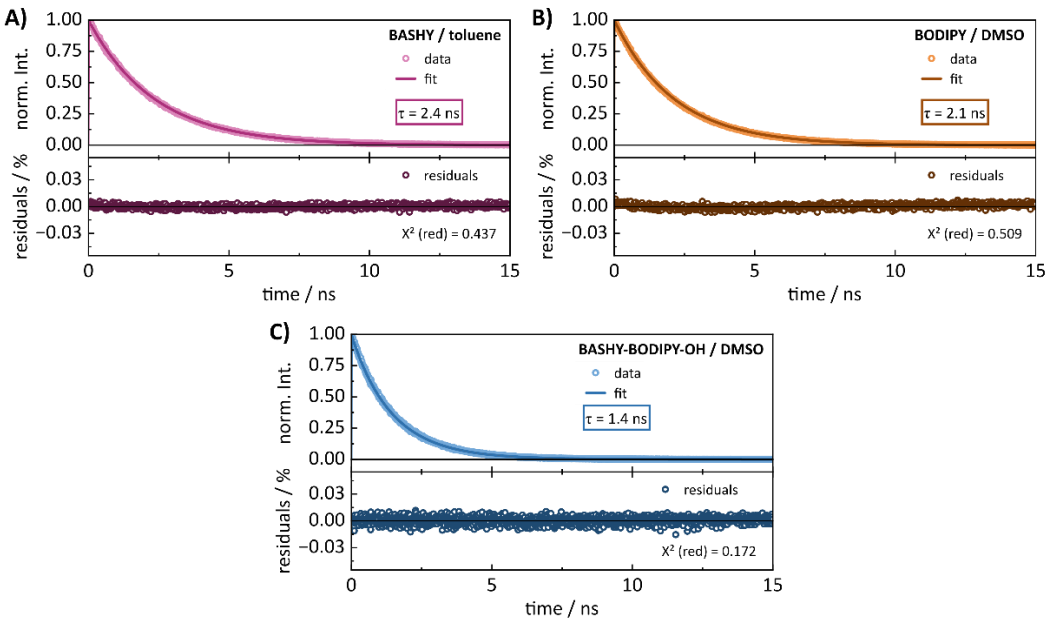

Figure S20. Fluorescence transients measured with our home-built TCSPC setup for A) BASHY in toluene, B) BODIPY in DMSO and C) BASHY-BODIPY-OH in DMSO. These measurements provide more precise excited-state lifetimes for these molecules, exceeding the measurement window of our transient absorption setup. The lifetimes, denoted within the boxes, are obtained by fitting the raw data with an exponential tailfit using the program FluoFit by PicoQuant. The qualities of the respective fits were evaluated by their X^2 values, which are all way below 1, making the obtained lifetimes valid. The lifetimes of BASHY and BODIPY were used to calculate the FRET rates (shown in Table 4 of the main text) for the different defined cases (presented in Figure 10 of the main text).

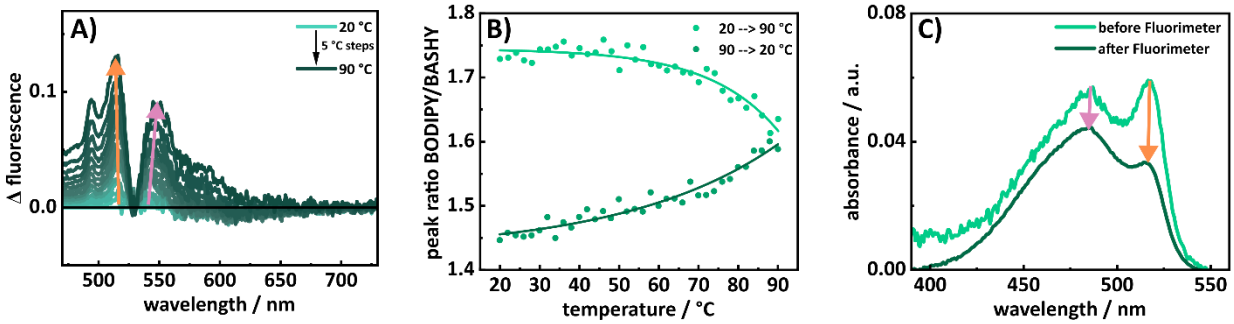

Figure S21. Temperature dependent fluorescence experiments of BASHY-BODIPY-SER. A) shows the difference fluorescence of the normalized spectra ranging from 20 to 90 °C. The spectra are normalized at 530 nm (main fluorescence peak). B) shows the ratio of BODIPY to BASHY maxima. From 20 to 55 °C, the ratio stays pretty constant. Around 60 °C a significant drop of the ratio starts and remains till the end temperature of 90 °C. Reversing the experiment from 90 to 20 °C reveals a mirror like behaviour. Instead of reaching the initial starting ratio, the ratio further drops. C) A comparison of the absorption spectra before and after the temperature experiment reveals that an uncaging or decomposition of the dyad took place.

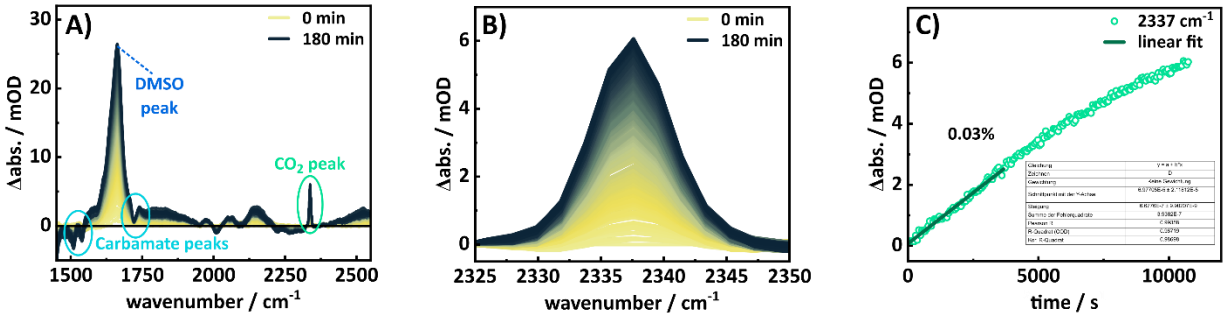

Figure S22. Uncaging experiments of BASHY-BODIPY-SER via illumination in the FTIR. A) shows the difference absorption spectra evolving from 0 up to 180 minutes. The spectra are shown from 1500 to 2500 cm^{-1} including the carbamate region and the CO_2 peak. While the CO_2 peak is pronounced quite well, the carbamate peaks are quite small and strongly hidden by the close lying DMSO peak. Due to increasing interactions between the molecule and the solvent during the illumination process, the solvent peaks strongly rise and conceal the molecule's peaks. Therefore, further assessments of the carbamate peaks were not possible. B) shows the same difference spectra, but zoomed into the CO_2 peak. C) shows the CO_2 evolution at 2337 cm^{-1} and the linear fit which was used to determine the uncaging quantum yield (0.03%) as described in the experimental section above.

6. NMR spectra

BODIPY 1

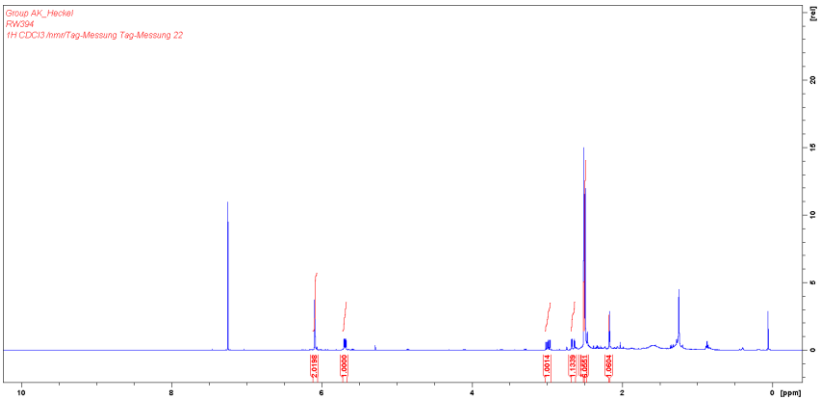

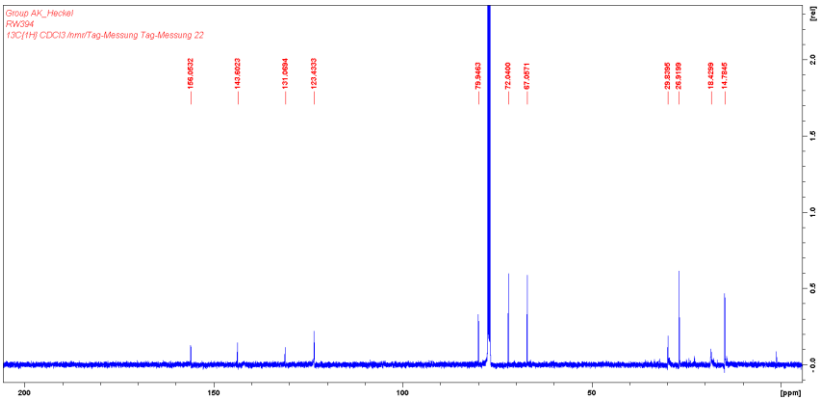

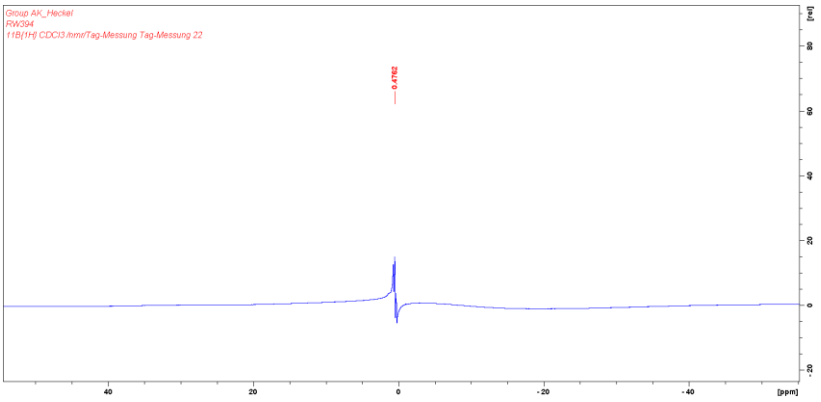

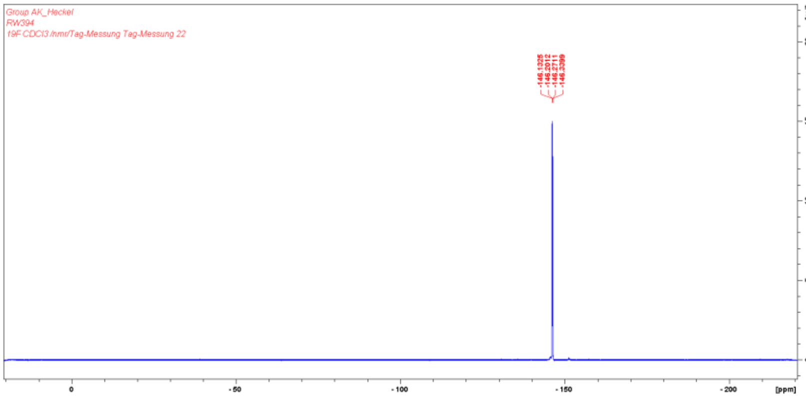
Group AK_Heckel
RW394
19F CDCl3 /nmr/Tag-Messung Tag-Messung 22

BASHY 2

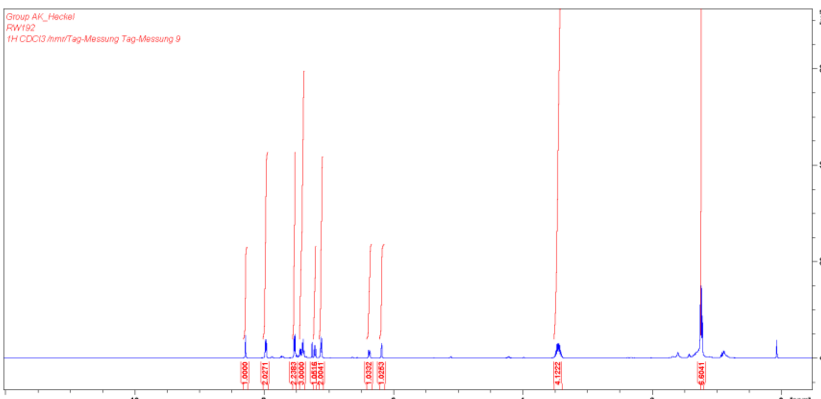
Group AK_Heckel
RW192
1H CDCl3 /nmr/Tag-Messung Tag-Messung 9

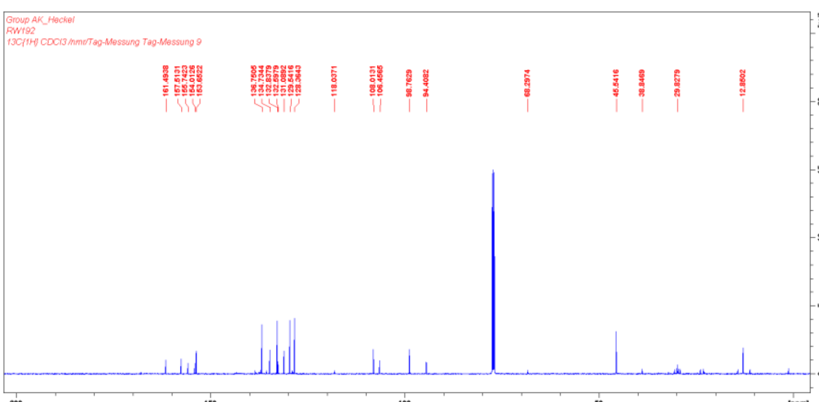
Group AK_Heckel
RW192
13C{1H} CDCl3 /nmr/Tag-Messung Tag-Messung 9

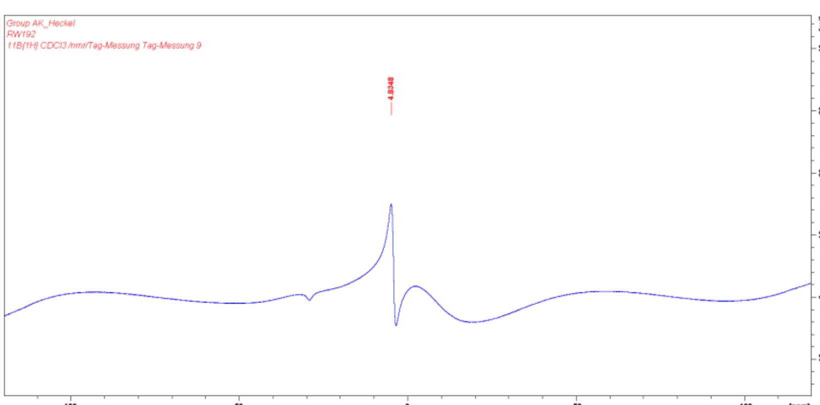
Group AK_Heckel
RW192
11B{1H} CDCl3 /nmr/Tag-Messung Tag-Messung 9

BASHY-BODIPY-OH

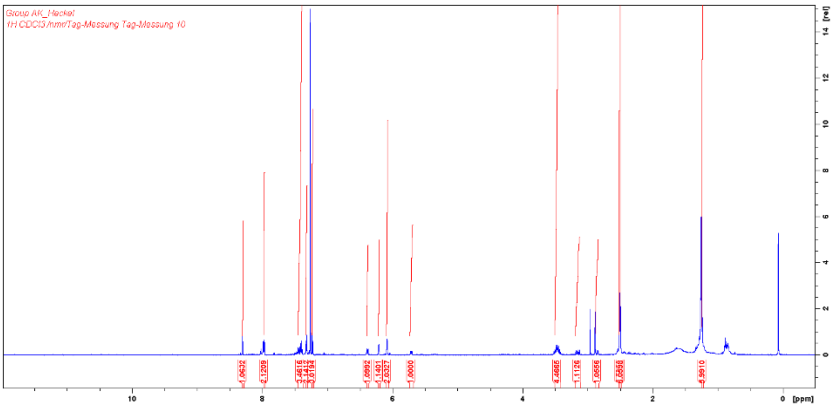

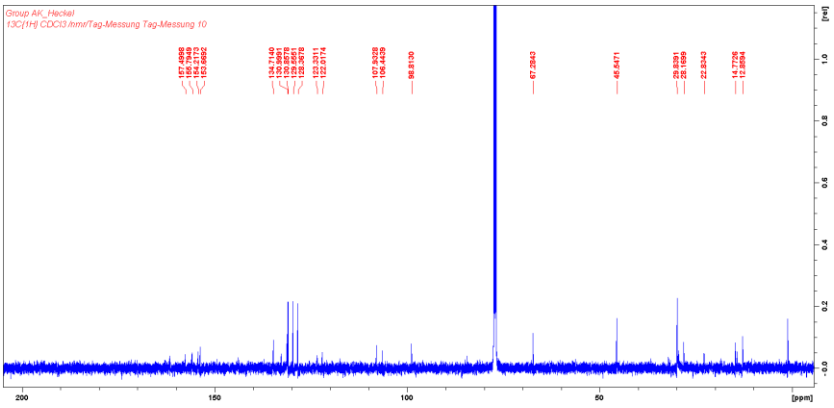

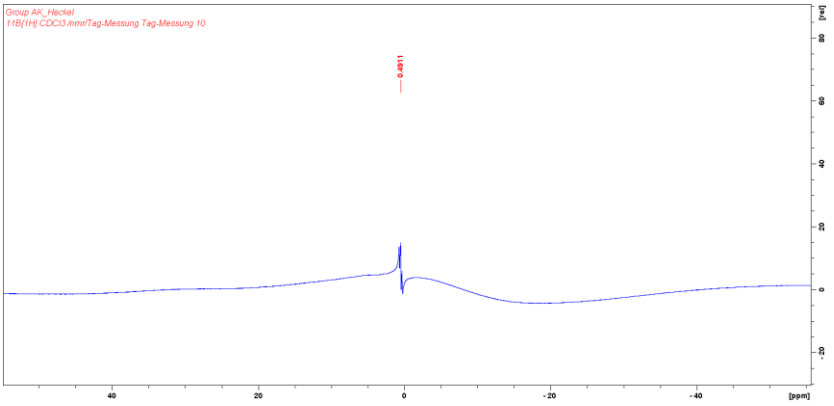

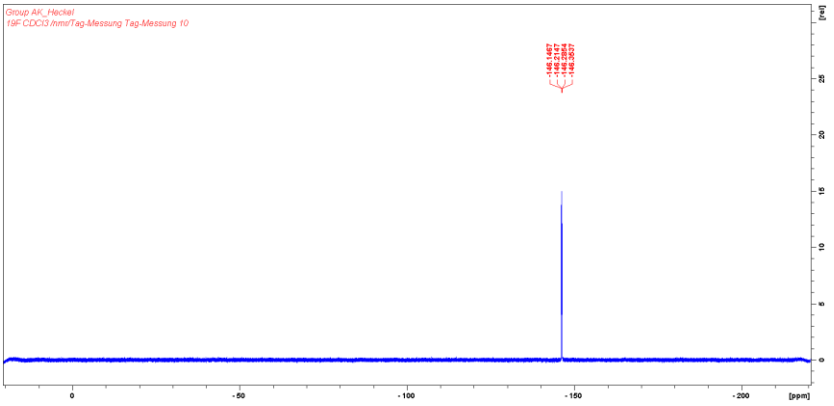

BASHY-BODIPY-SER

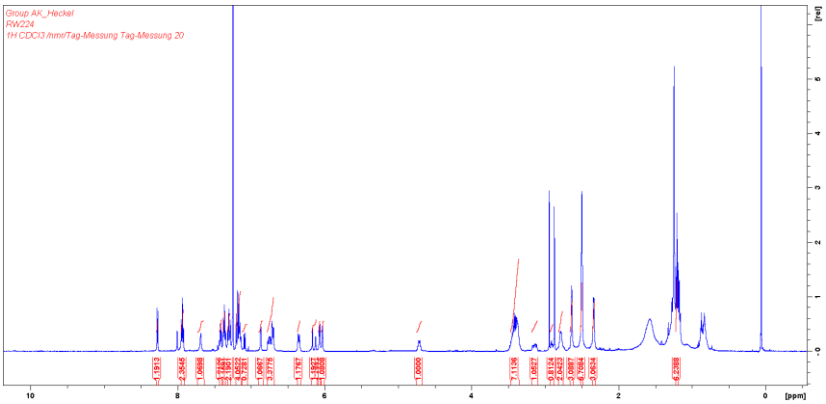

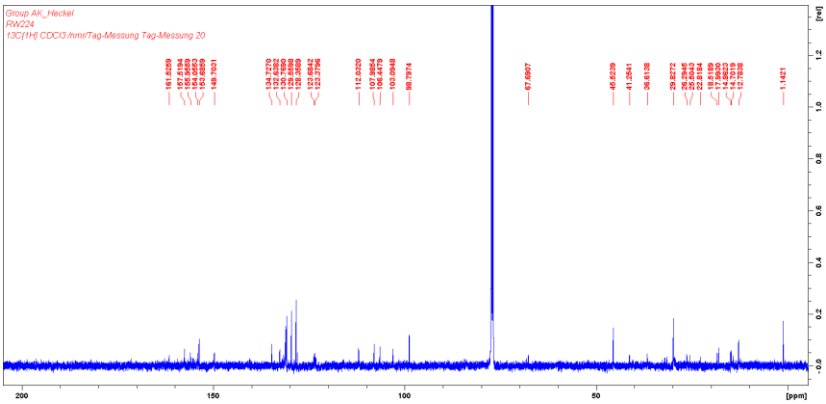

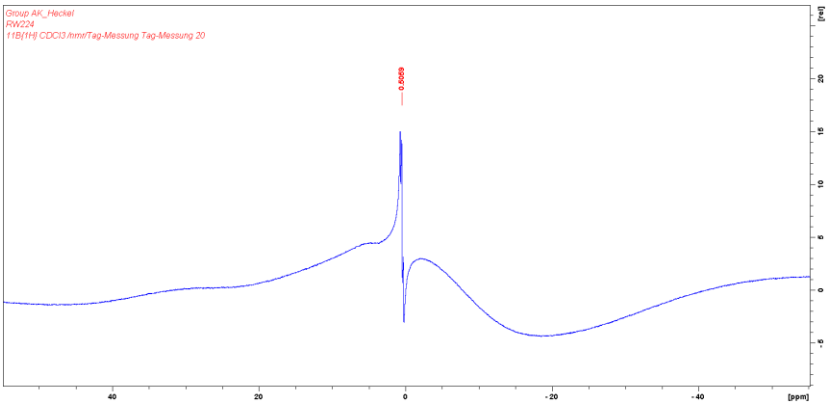

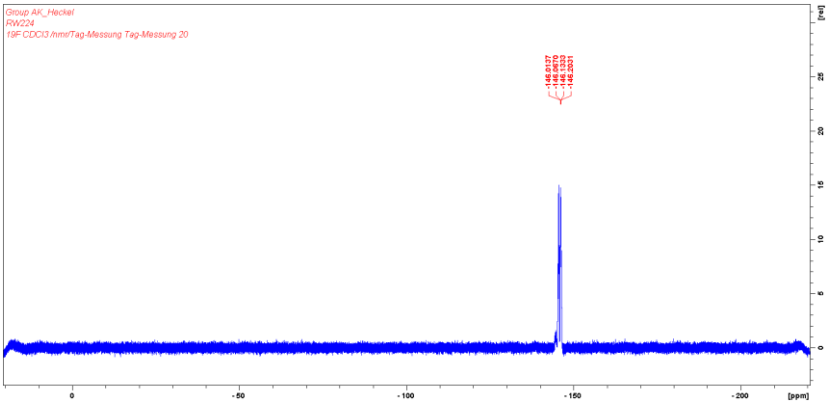

References

1 K. Krumova and G. Cosa, *J. Am. Chem. Soc.*, 2010, **132**, 17560–17569.
2 F. M. F. Santos, J. N. Rosa, N. R. Candeias, C. P. Carvalho, A. I. Matos, A. E. Ventura, H. F. Florindo, L. C. Silva, U. Pischel and P. M. P. Gois, *Chem. - Eur. J.*, 2016, **22**, 1631–1637.
3 N. S. Makarov, M. Drobizhev and A. Rebane, *Opt. Express*, 2008, **16**, 4029.
4 C. Slavov, H. Hartmann and J. Wachtveitl, *Anal. Chem.*, 2015, **87**, 2328–2336.
5 M. Falk and A. G. Miller, *Vib. Spectrosc.*, 1992, **4**, 105–108.
6 FRET (Förster or fluorescence resonance energy transfer), https://peternagyweb.hu/FRET.html, (accessed 28 October 2024).
7 Á. Szabó, J. Szöllősi and P. Nagy, *Curr. Protoc.*, 2022, **2**, e625.
8 M. J. Frisch, G. W. Trucks, H. B. Schlegel, G. E. Scuseria, M. A. Robb, J. R. Cheeseman, G. Scalmani, V. Barone, G. A. Petersson, H. Nakatsuji, X. Li, M. Caricato, A. V. Marenich, J. Bloino, B. G. Janesko, R. Gomperts, B. Mennucci, H. P. Hratchian, J. V. Ortiz, A. F. Izmaylov, J. L. Sonnenberg, D. Williams-Young, F. Ding, F. Lipparini, F. Egidi, J. Goings, B. Peng, A. Petrone, T. Henderson, D. Ranasinghe, V. G. Zakrzewski, J. Gao, N. Rega, G. Zheng, W. Liang, M. Hada, M. Ehara, K. Toyota, R. Fukuda, J. Hasegawa, M. Ishida, T. Nakajima, Y. Honda, O. Kitao, H. Nakai, T. Vreven, K. Throssell, J. A. Montgomery, Jr., J. E. Peralta, F. Ogliaro, M. J. Bearpark, J. J. Heyd, E. N. Brothers, K. N. Kudin, V. N. Staroverov, T. A. Keith, R. Kobayashi, J. Normand, K. Raghavachari, A. P. Rendell, J. C. Burant, S. S. Iyengar, J. Tomasi, M. Cossi, J. M. Millam, M. Klene, C. Adamo, R. Cammi, J. W. Ochterski, R. L. Martin, K. Morokuma, O. Farkas, J. B. Foresman, and D. J. Fox, *Gaussian16* Revision C.01. 2016.
9 S. Miertuš, E. Scrocco, and J. Tomasi, *Chem. Phys.* 1981, **55**, 117–129.
10 S. Miertuš and J. Tomasi, *Chem. Phys*. 1982, **65**, 239–245.
11 K. Aidas, C. Angeli, K. L. Bak, V. Bakken, R. Bast, L. Boman, O. Christiansen, R. Cimiraglia, S. Coriani, P. Dahle, E. K. Dalskov, U. Ekström, T. Enevoldsen, J. J. Eriksen, P. Ettenhuber, B. Fernández, L. Ferrighi, H. Fliegl, L. Frediani, K. Hald, A. Halkier, C. Hättig, H. Heiberg, T. Helgaker, A. C. Hennum, H. Hettema, E. Hjertenæs, S. Høst, I.-M. Høyvik, M. F. Iozzi, B. Jansik, H. J. Aa. Jensen, D. Jonsson, P. Jørgensen, J. Kauczor, S. Kirpekar, T. Kjærgaard, W. Klopper, S. Knecht, R. Kobayashi, H. Koch, J. Kongsted, A. Krapp, K. Kristensen, A. Ligabue, O. B. Lutnæs, J. I. Melo, K. V. Mikkelsen, R. H. Myhre, C. Neiss, C. B. Nielsen, P. Norman, J. Olsen, J. M. H. Olsen, A. Osted, M. J. Packer, F. Pawlowski, T. B. Pedersen, P. F. Provasi, S. Reine, Z. Rinkevicius, T. A. Ruden, K. Ruud, V. Rybkin, P. Salek, C. C. M. Samson, A. Sánchez de Merás, T. Saue, S. P. A. Sauer, B. Schimmelpfennig, K. Sneskov, A. H. Steindal, K. O. Sylvester-Hvid, P. R. Taylor, A. M. Teale, E. I. Tellgren, D. P. Tew, A. J. Thorvaldsen, L. Thøgersen, O. Vahtras, M. A. Watson, D. J. D. Wilson, M. Ziolkowski, and H. Ågren, "The Dalton quantum chemistry program system", *WIREs Comput. Mol. Sci.* 2014, **4**, 269–284.
12 F. Plasser, THEODORE: A package for theoretical density, orbital relaxation, and exciton analysis, 2019, http://theodore-qc.sourceforge.net.
13 F. Plasser, *J. Chem. Phys.*, 2020, **152**, 084108.
14 F. Plasser and H. Lischka, *J. Chem. Theory Comput.*, 2012, **8**, 2777–2789.
15 H. Tamura, R. Martinazzo, M. Ruckenbauer, and I. Burghardt, *J. Chem. Phys*. 2012, **137**, 22A540.
16 D. J. Tannor, Introduction to Quantum Mechanics: A Time-Dependent Perspective, *University Science Books: USA*, 1st edn, 2007.